Geoscience Frontiers xxx (xxxx) xxx

HOSTED BY

Contents lists available at ScienceDirect

China University of Geosciences (Beijing)

Geoscience Frontiers

journal homepage: www.elsevier.com/locate/gsf

Research Paper

Cretaceous tectonic evolution of the Neo-Tethys in Central Iran: Evidence from petrology and age of the Nain-Ashin ophiolitic basalts

Tahmineh Pirnia [a,*], Emilio Saccani [a], Ghodrat Torabi [b], Marco Chiari [c], Špela Goričan [d], Edoardo Barbero [a]

[a] Department of Physics and Earth Sciences, Ferrara University, Ferrara, 44122, Italy
[b] Department of Geology, Faculty of Science, University of Isfahan, Iran
[c] CNR, Istituto di Geoscienze e Georisorse, Florence, Italy
[d] Paleontološki inštitut Ivana Rakovca ZRC SAZU, Ljubljana, Slovenia

ARTICLE INFO

Article history:
Received 27 July 2018
Received in revised form
6 December 2018
Accepted 18 February 2019
Available online xxx

Keywords:
Ophiolite
Volcanic arc
Early Cretaceous
Nain
Ashin
Iran

ABSTRACT

The Nain and Ashin ophiolites consist of Mesozoic mélange units that were emplaced in the Late Cretaceous onto the continental basement of the Central-East Iran microcontinent (CEIM). They largely consist of serpentinized peridotites slices; nonetheless, minor tectonic slices of sheeted dykes and pillow lavas - locally stratigraphically associated with radiolarian cherts - can be found in these ophiolitic mélanges. Based on their whole rock geochemistry and mineral chemistry, these rocks can be divided into two geochemical groups. The sheeted dykes and most of the pillow lavas show island arc tholeiitic (IAT) affinity, whereas a few pillow lavas from the Nain ophiolites show calc-alkaline (CA) affinity. Petrogenetic modeling based on trace elements composition indicates that both IAT and CA rocks derived from partial melting of depleted mantle sources that underwent enrichment in subduction-derived components prior to melting. Petrogenetic modeling shows that these components were represented by pure aqueous fluids, or sediment melts, or a combination of both, suggesting that the studied rocks were formed in an arc-forearc tectonic setting. Our new biostratigraphic data indicate this arc-forearc setting was active in the Early Cretaceous. Previous tectonic interpretations suggested that the Nain ophiolites formed, in a Late Cretaceous backarc basin located in the south of the CEIM (the so-called Nain-Baft basin). However, recent studies showed that the CEIM underwent a counter-clockwise rotation in the Cenozoic, which displaced the Nain and Ashin ophiolites in their present day position from an original northeastward location. This evidence combined with our new data and a comparison of the chemical features of volcanic rocks from different ophiolites around the CEIM allow us to suggest that the Nain-Ashin volcanic rocks and dykes were formed in a volcanic arc that developed on the northern margin of the CEIM during the Early Cretaceous in association with the subduction, below the CEIM, of a Neo-Tethys oceanic branch that was existing between the CEIM and the southern margin of Eurasia. As a major conclusion of this paper, a new geodynamic model for the Cretaceous evolution of the CEIM and surrounding Neo-Tethyan oceanic basins is proposed.

1. Introduction

The geology of Iran is characterized by the outstanding occurrence of a number of ophiolitic complexes (Fig. 1a). A few of them represent remnants of the Paleo-Tethys Ocean and mainly crop out in northern Iran along the Alborz Range (Lensch and Davoudzadeh, 1982). However, most of the Iranian ophiolites are Mesozoic in age and record the complex and long-lived geodynamic history of the different branches of the Neo-Tethys that developed between the Arabian plate and the composite puzzle of microplates, which characterized the southern margin of the Eurasian continent from Late Triassic to early Cenozoic (e.g., Desmons and Beccaluva, 1983; Sengör, 1990; Barrier and Vrielynck, 2008). The Iranian Mesozoic ophiolites have classically been divided into three major belts (Stöcklin, 1974; Lensch and Davoudzadeh, 1982) (Fig. 1a): (1)

* Corresponding author.
E-mail address: tahmineh.pirnia@gmail.com (T. Pirnia).
Peer-review under responsibility of China University of Geosciences (Beijing).

https://doi.org/10.1016/j.gsf.2019.02.008

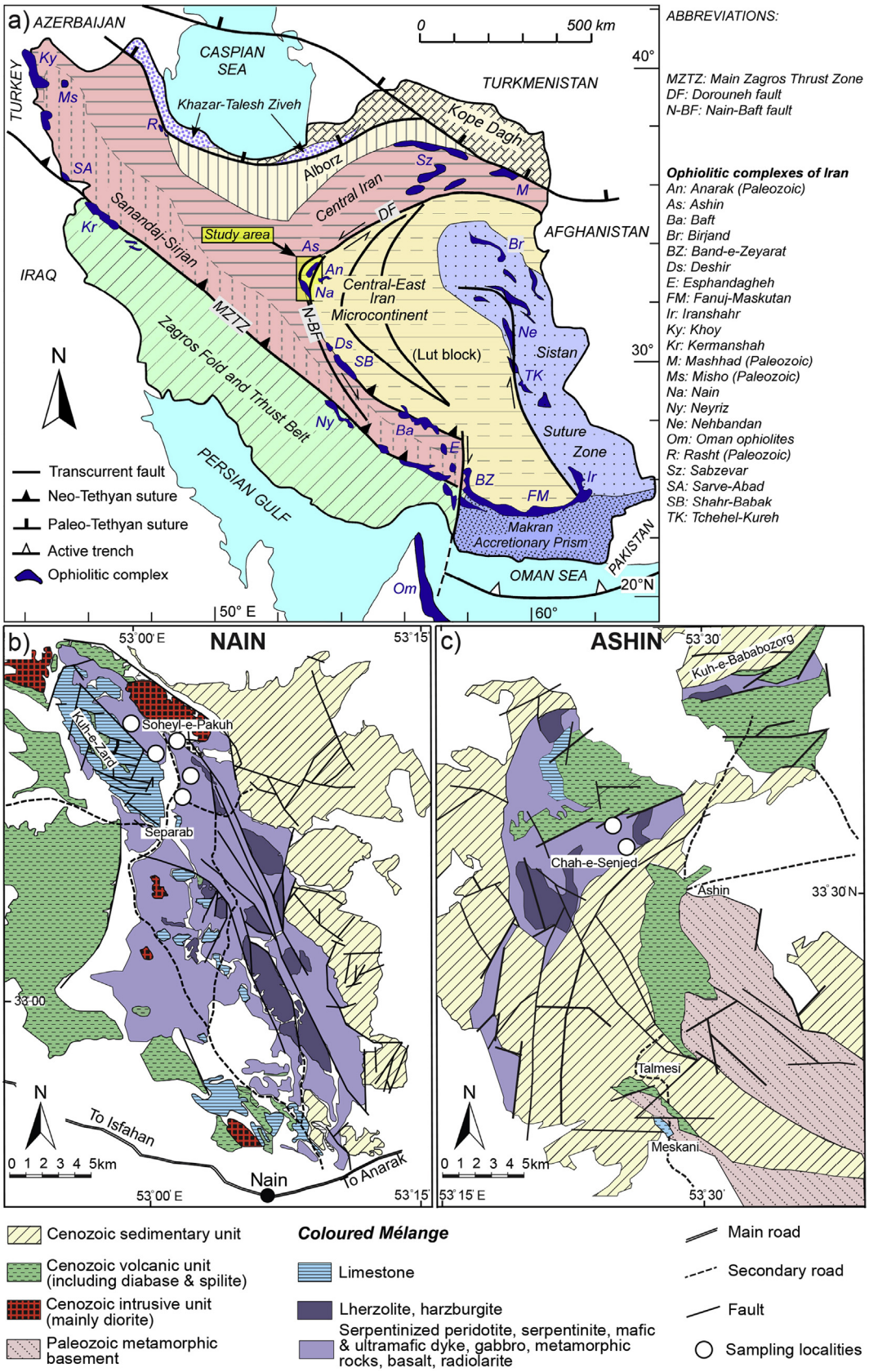

Figure 1. (a) Geological map of Iran. Ophiolites and major tectonic units are shown. (b) Simplified geological map of the Nain ophiolitic mélange (modified after Davoudzadeh, 1972). (c) Simplified geological map of the Ashin ophiolitic mélange (modified from the Anarak geological map 1:250,000, Sharkovski et al., 1984). Sample locations are shown.

Please cite this article as: Pirnia, T et al., Cretaceous tectonic evolution of the Neo-Tethys in Central Iran: Evidence from petrology and age of the Nain-Ashin ophiolitic basalts, Geoscience Frontiers, https://doi.org/10.1016/j.gsf.2019.02.008

ophiolites of the Zagros suture belt representing remnants of the Southern Neo-Tethys, which opened during the Triassic between the Arabian plate and the Central Iran continental block (e.g., Robertson, 2007, and references therein); (2) ophiolites of the Makran accretionary prism, which includes the incomplete ophiolitic sequences and ophiolitic mélanges of Band-e-Zeyarat, Dar Anar, and Fanuj-Maskutan (e.g., McCall, 2002; Delavari et al., 2016; Saccani et al., 2017a); (3) ophiolites and ophiolitic mélanges (the so called "Coloured Mélanges") that mark the boundaries of the Central-East Iranian microcontinent (CEIM). These include the Sabzevar ophiolites in the north, the Nain, Dehshir, Shahr-e-Babak, Baft ophiolites (or, simply, the Nain-Baft ophiolitic belt) in the southwest, and the Sistan zone ophiolites in the east of the CEIM (e.g., Camp and Griffis, 1982; Ghazi and Hassanipak, 2000; Shojaat et al., 2003; Rahmani et al., 2007; Shafaii Moghadam et al., 2009; Rossetti et al., 2010; Saccani et al., 2010; Angiboust et al., 2013; Omrani et al., 2013; Rezaei et al., 2018). The Nain and Ashin ophiolites are of particular interest as they crop out at the westernmost corner of the CEIM, which is marked in this area by the intersection of two major regional-scale fault systems, namely, the Nain-Baft and the Dorouneh (also known as Great Kavir-Dorouneh) fault systems (Fig. 1a). They consist of ophiolitic mélange units ("Coloured Mélange") that were emplaced during Late Cretaceous–lower Paleocene times onto the continental basement of the CEIM (Davoudzade, 1972; Stöcklin, 1974; Stoneley, 1975). Several studies have been carried out on these ophiolites. However,

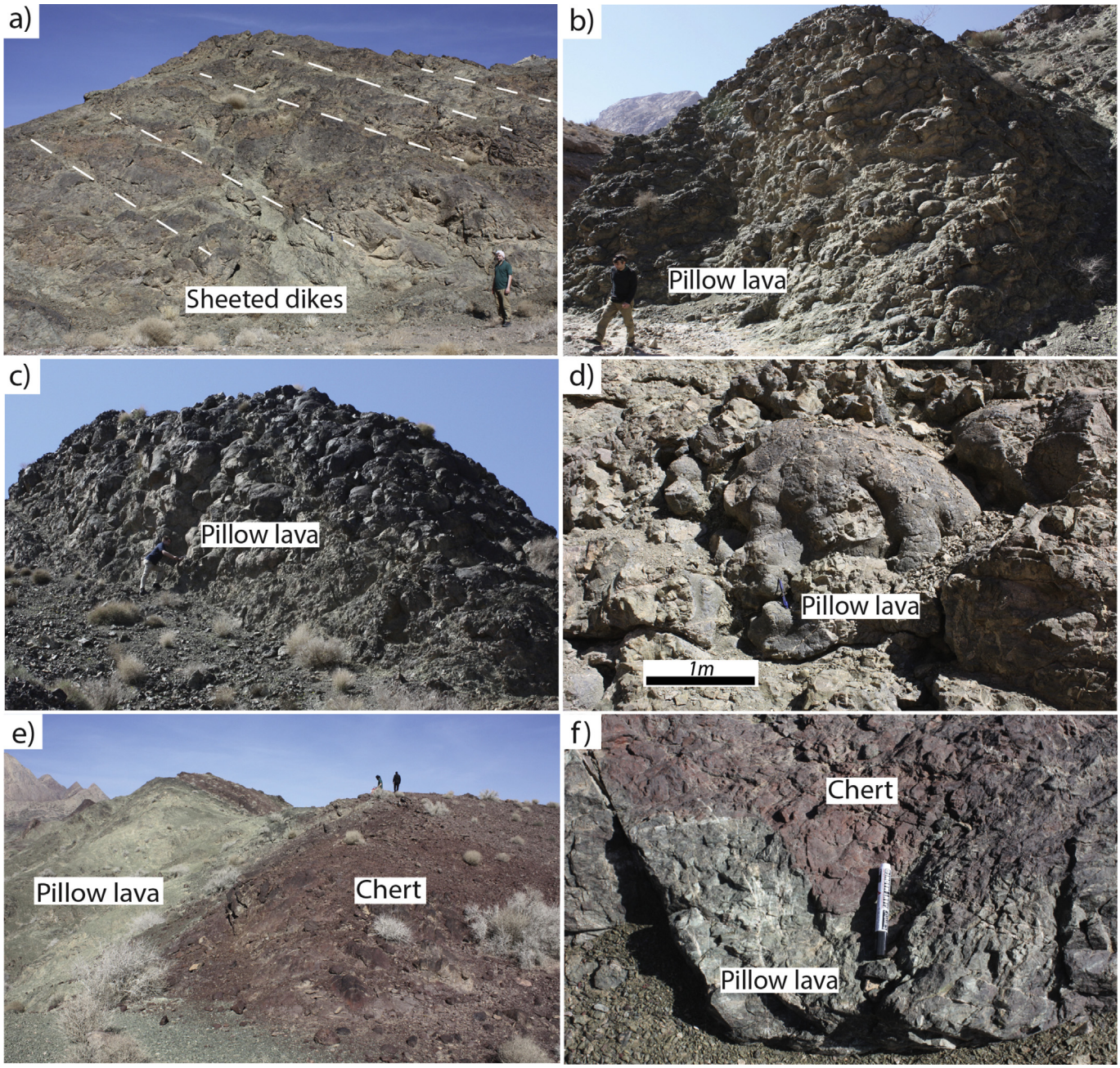

Figure 2. Field photographs of the upper crust ophiolitic rocks in the Nain and Ashin ophiolites. (a) Sheeted dyke outcrop in the Nain ophiolite. The dashed lines show the general trend of dykes; (b, c) pillow lavas in the Nain and Ashin ophiolites, respectively; (d) close view of the basaltic pillow lavas in the Nain area; (e) stratigraphic contact between pillow lavas and radioralian cherts in the Ashin ophiolites; (f) close view of the contact shown in Fig. 2e.

Please cite this article as: Pirnia, T et al., Cretaceous tectonic evolution of the Neo-Tethys in Central Iran: Evidence from petrology and age of the Nain-Ashin ophiolitic basalts, Geoscience Frontiers, https://doi.org/10.1016/j.gsf.2019.02.008

no general consensus still exists on their tectono-magmatic implication, and different hypotheses have been suggested about the nature and geodynamic significance of the oceanic branch in which they were formed. Some authors have indicated a supra-subduction zone (SSZ) geochemical affinity for the Nain ophiolites, as well as for the neighboring Shahr-e-Babak ophiolites, and suggested that they were formed in an intra-oceanic island arc setting during the Late Cretaceous (e.g., Ghazi and Hassanipak, 2000; Rahmani et al., 2007). Geochemical studies on the mafic lavas of the Nain and Dehshir ophiolites (Shafaii Moghadam et al., 2008, 2009), as well as on the mantle peridotites (Mehdipour Ghazi et al., 2010; Pirnia et al., 2010) have suggested that the Nain-Baft ophiolites were originated in a backarc basin, which opened between the Sanandaj-Sirjan zone and the CEIM in the Late Cretaceous in response to the subduction of the Southern Neo-Tethys below the Sanandaj-Sirjan block (see Takin, 1972; McCall, 2002; Shahabpour, 2005; Barrier and Vrielynck, 2008). However, a recent petrological study has suggested that mantle lherzolites in the Nain ophiolites represent sub-continental mantle exhumed at an Iberia-type ocean-continent transition zone (Pirnia et al., 2018) and a recent biostratigraphic study has shown that the Ashin ophiolites are mid Cretaceous in age (Shirdashtzadeh et al., 2015).

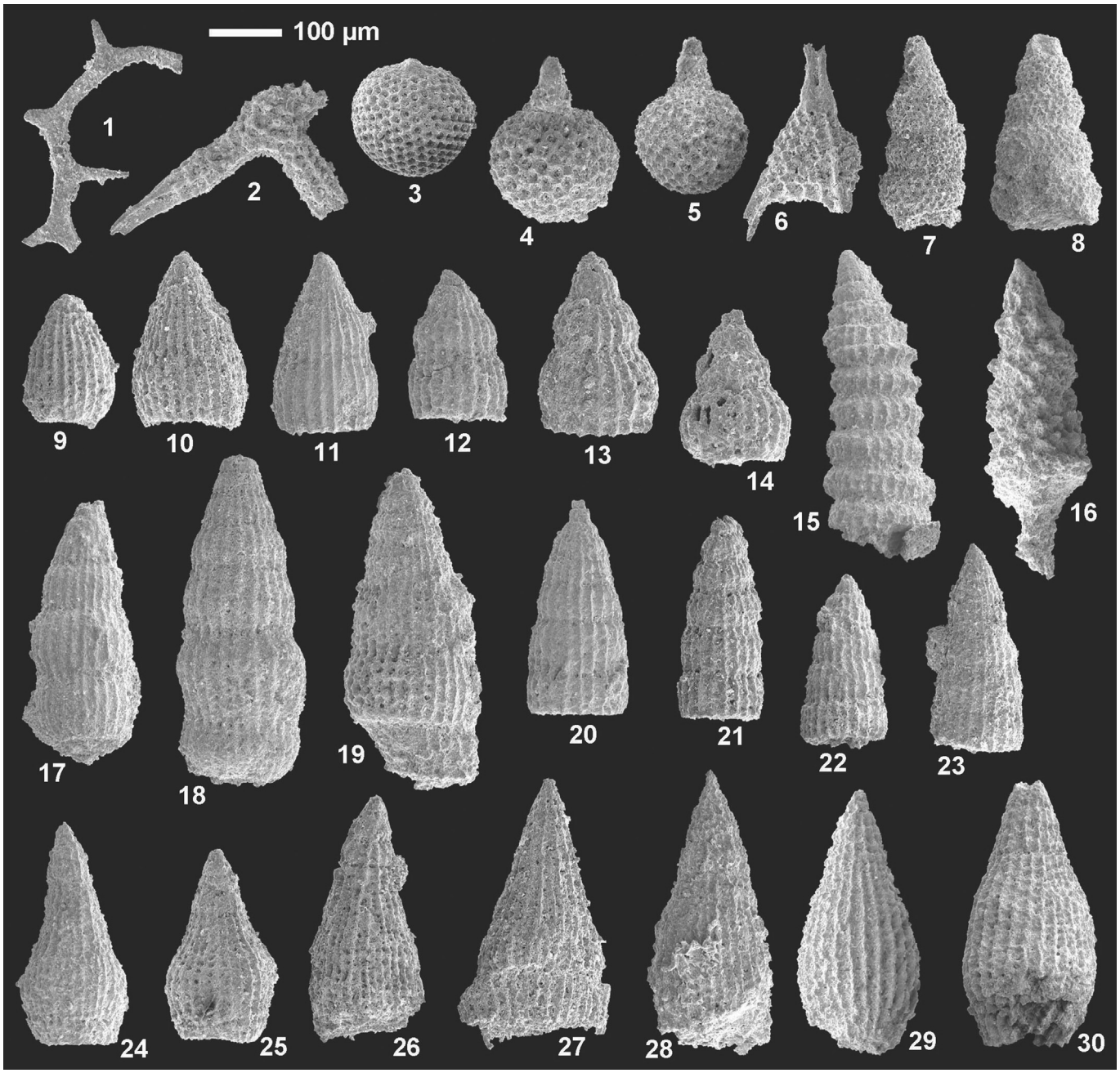

Figure 3. Albian radiolarians from sample 1010, magnification of all specimens 120× (scale bar 100 µm). 1. *Acanthocircus* cf. *levis* (Donofrio and Mostler); 2. *Crucella* cf. *euganea* (Squinabol); 3. *Cryptamphorella conara* (Foreman); 4, 5. *Crococapsa asseni* (Tan); 6. *Napora* cf. *praespinifera* (Pessagno); 7, 8. *Parvimitrella communis* (Squinabol); 9, 10. *Thanarla brouweri* (Tan); 11, 12. *Thanarla praeveneta* Pessagno; 13, 14. *Thanarla* aff. *praeventa* Pessagno. This morphotype has stronger constrictions than typical *Thanarla praeveneta*. In the studied sample, *Thanarla brouweri* and *Thanarla* aff. *praeventa* are two end members linked by a continuum of transitional forms (*Thanarla praeveneta*) with indistinct morphological delimitations; 15. *Pseudodictyomitra* cf. *paronai* (Aliev); 16. *Xitus* cf. *spicularius* (Aliev); 17–23. *Dictyomitra montisserei* (Squinabol) *sensu* O'Dogherty (1994); 24–30. *Mita gracilis* (Squinabol).

Please cite this article as: Pirnia, T et al., Cretaceous tectonic evolution of the Neo-Tethys in Central Iran: Evidence from petrology and age of the Nain-Ashin ophiolitic basalts, Geoscience Frontiers, https://doi.org/10.1016/j.gsf.2019.02.008

In addition, recent paleomagnetic studies have shown that the CEIM underwent significant counter-clockwise rotation of about 30° during the Late Jurassic–Early Cretaceous and again after the Middle–Late Miocene (Mattei et al., 2012, 2014). As a consequence, it is reasonable to hypothesize that the Nain and Ashin ophiolites were displaced in their present day position by the rotation of the CEIM, implying that they were formed in an oceanic sector that was located during the mid Cretaceous to the northeast with respect their current position. These recent studies show robust evidence in contrast to the most accepted hypothesis of formation of the Nain and Ashin ophiolites in the Nain-Baft backarc basin in the southwest of the CEIM (Barrier and Vrielynck, 2008; Shafaii Moghadam et al., 2009). For this reason, we present new whole rock geochemical and petrological data, as well as mineral chemistry data on sheeted dykes and pillow lavas from the Nain and Ashin ophiolitic complexes with the aim of constraining their petrogenetic processes and their tectono-magmatic setting of formation. We also present new biostratigraphic data on radiolarian cherts stratigraphically associated with the studied pillow lavas. These data will allow the type and age of the magmatic events to be constrained in detail. Several models for the geodynamic evolution of the oceanic branches of the Neo-Tethys that existed in Mesozoic times around the CEIM are available in literature (e.g., Shojaat et al., 2003; Barrier and Vrielynck, 2008; Shafaii Moghadam et al., 2009; Rossetti et al., 2010; Omrani et al., 2013; Mattei et al., 2014; Shirdashtzadeh et al., 2015). Hence, one of the main goals of this paper is to use our new data for testing and developing the extant tectonic models. We anticipate that the data presented herein allow us to propose a new model for the tectonic evolution of the CEIM and surrounding oceanic seaways during the Cretaceous.

2. Geological setting, field evidence, and sampling

2.1. General geological setting

The Nain and Ashin ophiolites are located in the northeast of the Isfahan Province in Central Iran (Fig. 1a). These ophiolites are emplaced onto the westernmost corner of the CEIM, which is defined in this area by the intersection of two major regional-scale fault systems, namely, the Nain-Baft and the Dorouneh fault systems (Fig. 1a). These ophiolites were classically considered as part of the Mesozoic, discontinuous ophiolitic belt that surround the northern, western, and southern borders of the CEIM (Lensch and Davoudzadeh, 1982). In fact, this ophiolitic belt also includes the Sabzevar ophiolites, to the north and the Dehshir and Baft ophiolites, to the southwest (Fig. 1a).

The Nain and Ashin ophiolitic complexes both consist of an ophiolitic mélange (also known as “Coloured Mélange”) including relics of the Mesozoic Neo-Tethys Ocean that were emplaced onto the CEIM continental margin in Late Cretaceous–lower Paleocene (e.g., Davoudzadeh, 1972; Torabi et al., 2011a, b). The Nain and Ashin ophiolitic mélanges both include very similar rock assemblages, and are formed by tectonic slices or blocks of different types of ophiolitic and metaophiolitic rocks (Fig. 1b and c). Mantle peridotites largely prevail in volume. They consist of serpentinites, harzburgites, and lherzolites generally showing a marked foliation

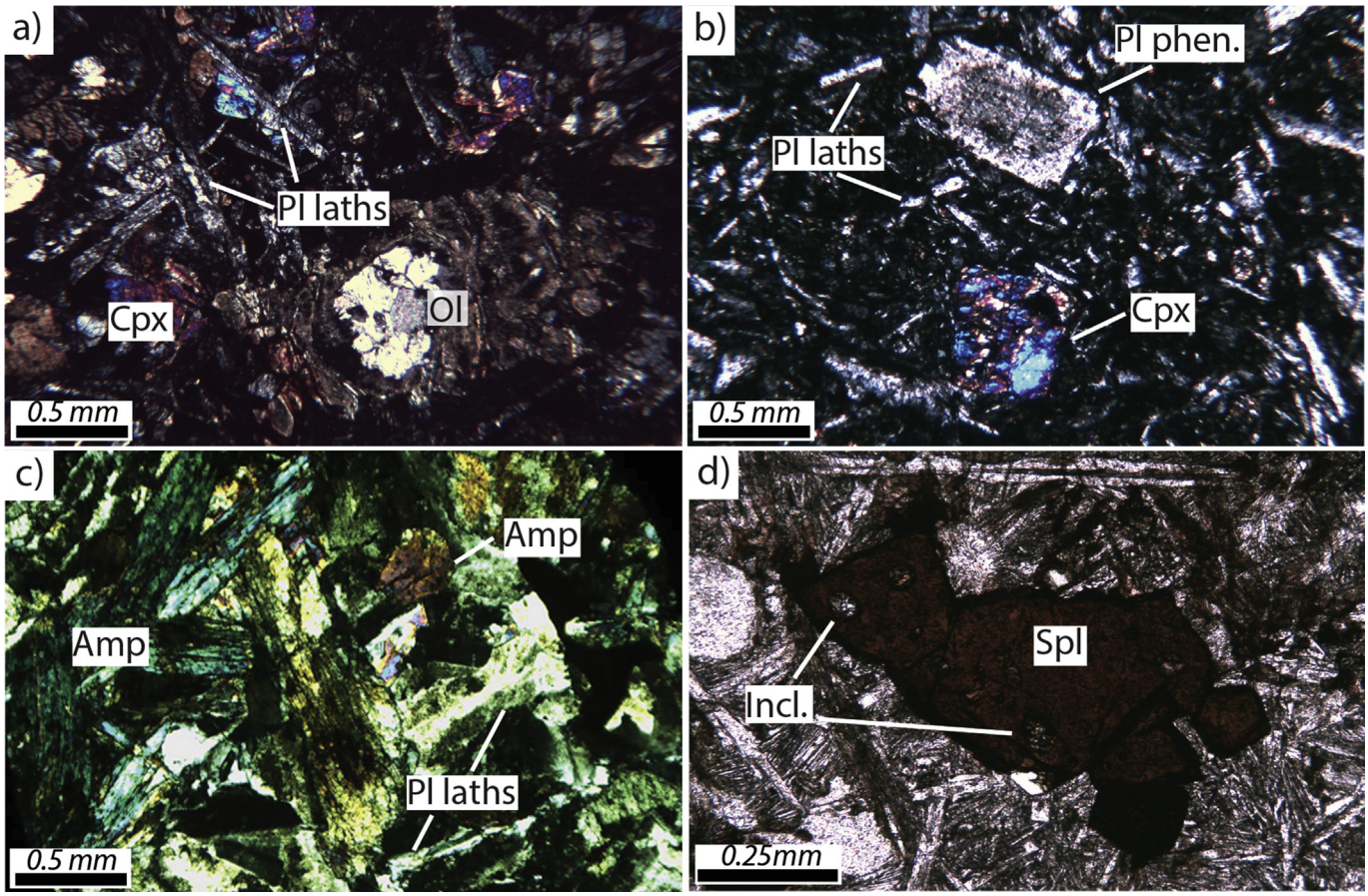

Figure 4. Photomicrographs of the pillow lavas and dykes from the Nain and Ashin ophiolites. (a) Olivine (Ol) phenocryst in a groundmass with intersertal texture composed of plagioclase (Pl) laths and intergranular clinopyroxene (Cpx), and minor glass (Nain pillow lava, sample NA407); (b) phenocrysts of Cpx and Pl in a groundmass showing subophitic texture (Nain pillow lava, sample 229); (c) coarse-grained doleritic texture with Pl and hornblende amphibole (Amp) in the Nain sheeted dykes (sample NA538); (d) euhedral chromian-spinel (Spl) showing inclusions of altered silicate minerals (Incl.) in the Ashin pillow lavas. (a–c): Cross polarized light; (d): plane polarized light.

Please cite this article as: Pirnia, T et al., Cretaceous tectonic evolution of the Neo-Tethys in Central Iran: Evidence from petrology and age of the Nain-Ashin ophiolitic basalts, Geoscience Frontiers, https://doi.org/10.1016/j.gsf.2019.02.008

(Pirnia et al., 2010, 2013, 2014). Harzburgites locally include subordinate amounts of dunites and podiform chromitites, as well as several dykes of pyroxenites, wehrlites and rodingites (Davoudzadeh, 1972). Pirnia et al. (2018) have recently shown that most lherzolites represent sub-continental type mantle, which is very similar to that cropping out in the Alpine Tethys ophiolites. These authors have suggested that, similar to the Alpine Tethys ophiolites (see Saccani et al., 2015), these lherzolites represent sub-continental mantle exhumed, through an asymmetric passive extension, during the continental breakup that preceded the oceanic formation.

Crustal rocks are very subordinate in volume. The scarce intrusive rocks are represented by pegmatitic and isotropic gabbros, diorites, gabbronorites, always occurring as small-sized bodies and dykes within the mantle peridotites. Plagiogranites, sheeted dykes (Fig. 2a) and pillow lavas (Fig. 2b–d) are found as distinct slices in tectonic contact with the mantle sequences. Pillow lavas are commonly stratigraphically covered by pelagic sedimentary rocks, which clearly indicate that they were erupted in a sub-marine environment. These pelagic sedimentary rocks are represented by radiolarian cherts (Fig. 2e and f) and Campanian–Maastrichtian Globotruncana limestones (Davoudzadeh, 1972). All magmatic crustal rocks underwent spilitization and sea floor metamorphisms (Torabi et al., 2008). Pillow lavas are mostly found close to the sheeted dykes, but not in stratigraphic contact, in the western part of the Nain ophiolites and in the eastern side of the Ashin ophiolites (Fig. 1b and c). In the Nain ophiolites, they are discontinuously exposed along a N–S trend in the southwest of Soheyl-e-Pakuh and near Separab (Rahmani et al., 2007) (Fig. 1b). The sheeted dyke complex cover an area of about 5 km^2 and the thickness of single dykes ranges from 10 cm to 3 m (Rahmani et al., 2007). Dykes locally cut high-level amphibole gabbros and plagiogranites. The pillow lavas form thin individual tectonic slices that can reach up to 10 m in thickness. In the Ashin ophiolite, sheeted dykes and pillow lavas crop out near Chah-e-Senjed (Fig. 1c). Similar to the Nain ophiolite, pillow lavas slices are relatively thin; they reach ~25 m in thickness, on average (Torabi, 2004). A K-Ar age of 98 Ma determined on plagiogranites (Sharkovski et al., 1984) suggests a Cenomanian age for the formation of the intrusive rocks from the Ashin ophiolite. In addition, $^{40}Ar/^{39}Ar$ ages ranging from 101.2 ± 0.9 Ma to 99 ± 1.2 Ma have been determined for one hornblende-gabbro (Hassanipak and Ghazi, 2000). Unfortunately, no indication is given by these authors about the geochemical nature (i.e., subduction-related or subduction-unrelated) of the dated gabbro.

In both ophiolitic mélanges, metaophiolitic rocks include metagabbros, metaplagiogranites, amphibolites, banded metacherts, and successions of marbles and schists (Sharkovski et al., 1984; Shirdashtzadeh et al., 2010). Shirdashtzadeh et al. (2010) and Torabi et al. (2011b) suggested that the protholiths of the amphibolitic rocks from both Nain and Ashin ophiolites were represented by diabasic dykes and basaltic pillow lavas both showing normal mid-ocean ridge affinity (N-MORB). However, Shirdashtzadeh et al. (2011) also proposed an IAT affinity for the amphibolites. According to these authors, metacherts and marble-schists successions can be regarded as the original sedimentary cover of the pillow lava basalts. Shirdashtzadeh et al. (2010) suggested that the metamorphic slices included within the Nain and Ashin mélanges represent relics a Jurassic oceanic crust that underwent a Late Cretaceous metamorphic event (Shafaii Moghadam et al., 2009).

Cenozoic volcanic rocks associated with small coeval dioritic intrusions, as well as Cenozoic sedimentary rocks extensively crop out in both Nain and Ashin areas (Davoudzadeh, 1972). However, in the Nain area, the volcanic and sedimentary rocks are separated and crop out to the west and to the east of the ophiolitic mélange, respectively (Fig. 1b). In contrast, in the Ashin area, Cenozoic sedimentary rocks largely prevail and entirely surround the ophiolitic mélange, whereas Cenozoic volcanic rocks locally crop out on the top of the ophiolitic mélange, as well as to the east of the Tertiary sedimentary succession (Fig. 1c). In addition, in the Ashin area, Paleozoic metamorphic rocks, including metaophiolitic rocks (Anarak Complex) largely crop out in the easternmost side (Zanchi et al., 2015; Berra et al., 2017; Zanchetta et al., 2017) (Fig. 1c). It has been suggested that the emplacement of both Nain and Ashin Mesozoic ophiolitic mélanges onto the CEIM occurred before Paleocene times, since they are unconformably covered by Paleocene–Eocene sedimentary rocks (Davoudzade, 1972). However, some authors suggested that their emplacement took place in the Late Cretaceous (Stöcklin, 1974; Stoneley, 1975).

Rahmani et al. (2007) have suggested that the Nain sheeted dykes display island arc tholeiitic (IAT) affinity and concluded that their formation is related to an intra-oceanic SSZ setting. However, other authors suggested that ophiolitic rocks from both Nain and Ashin ophiolitic mélanges were originated in a back-arc basin setting (e.g., Torabi et al., 2008; Shafaii Moghadam et al., 2009; Pirnia et al., 2010, 2014).

2.2. Field evidence and sampling

Sampling was focused on the mafic sheeted dykes and pillow lavas cropping out as distinct tectonic slices in the Nain and Ashin ophiolitic mélanges. Radiolarian cherts showing clear stratigraphic contacts with pillow lavas have also been sampled in some localities in order to constrain the age of the associated pillow lavas in detail.

In the Nain area (Fig. 1b), a total of four sheeted dyke, fourteen pillow lava, and six radiolarian chert samples were collected from the ophiolitic mélange. Sheeted dykes were sampled along the road from Separab to Soheyl-e-Pakuh. In this locality, dykes show variable thickness, ranging from 0.5 to 3 m (Fig. 2a). They form a small (some tens of meters) tectonic slice juxtaposed onto a thick harzburgite slice. Pillow lavas were collected in some distinct tectonic slices cropping out in the neighborhood of Soheyl-e-Pakuh, mainly in the northwest of this village. In a couple of these tectonic slices, pillow lavas are stratigraphically covered by radiolarian cherts. The thicknesses of these slices are difficult to be determined because

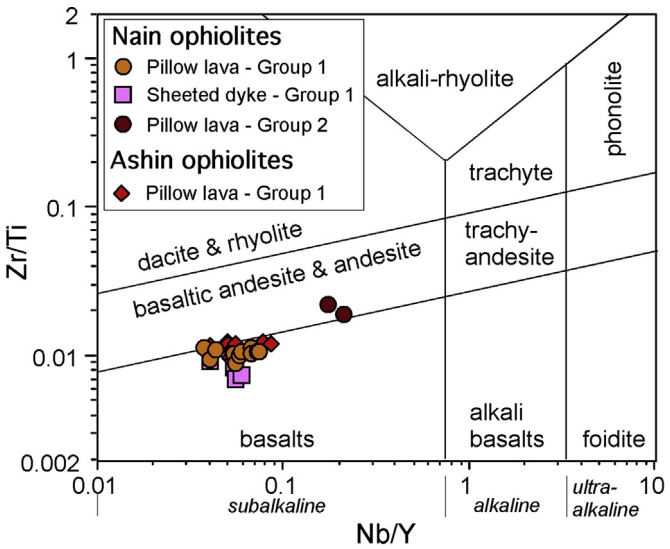

Figure 5. Nb/Y vs. Zr/Ti discrimination diagram of Winchester and Floyd (1977) modified by Pearce (1996) for basaltic pillow lavas and sheeted dykes of the Nain and Ashin ophiolites.

Please cite this article as: Pirnia, T et al., Cretaceous tectonic evolution of the Neo-Tethys in Central Iran: Evidence from petrology and age of the Nain-Ashin ophiolitic basalts, Geoscience Frontiers, https://doi.org/10.1016/j.gsf.2019.02.008

their boundary contacts are poorly exposed due to a widespread Quaternary sedimentary cover. However, their thickness can be estimated to be from 10 to 50 m and they generally lie onto the top of mantle peridotites. Pillow lavas commonly show spherical to elliptical shapes (Fig. 2b), thought tubular and irregular shapes can also be seen. The interstitial spaces between the pillows are often filled by hyaloclastite breccia (Fig. 2d) and, rarely, by interpillow radiolarian cherts. The pillows are very variable in size, ranging from 0.2 to 2 m in diameter. The pillow lava series are locally cross-cut by deeply altered individual dykes of variable nature. In the tectonic slices consisting of pillow lava-radiolarian chert sequences, the contact between pillow lava and overlying radiolarian cherts can be abrupt or transitional depending on localities. The transitional contact is characterized by lenses and patches of chert embedded in the top of the pillow lava series and vice versa by pillow lava lenses embedded in the bottom of the radiolarian chert sequences. The radiolarian cherts are characterized by a red-brownish color. The radiolarian cherts generally show layering with very variable thickness (1–5 cm) or massive bedding. The thickness of radiolarian chert sequences ranges from 10 to 40 m. Radiolarian cherts were taken from both the tectonic slices consisting of pillow lava-radiolarian chert sequences. In detail, radiolarian cherts NA424 and NA425 were stratigraphically associated with pillow lava sample NA421, whereas radiolarian cherts NA501, NA502, NA503, and NA510 were associated with pillow lava NA509.

In the Ashin ophiolite, a total of ten samples of pillow lavas, and three samples of radiolarian cherts were taken from the ophiolitic mélange. Sheeted dykes where sampled in small and tectonized outcrops. In fact, after preliminary petrographical and chemical analyses they resulted totally altered and therefore they will not be treated in this paper. Pillow lavas were collected in two distinct tectonic slices cropping out in the Chah-e-Senjed area (Fig. 1c) where the best preserved outcrops are found. Pillow lavas show general features that are very similar to those of pillow lavas in the Nain ophiolite (Fig. 2c). Similar to Nain ophiolite, the thicknesses of the tectonic slices made up of pillow lava or pillow lava-radiolarian chert sequences are difficult to be determined, but it can be estimated to be about 25 m for pillow lavas and about 50 m for pillow lava-radiolarian chert sequences (Fig. 2e). These tectonic slices are found onto the top of mantle peridotites. In the pillow lava-radiolarian chert sequences, the contact between pillow lava and

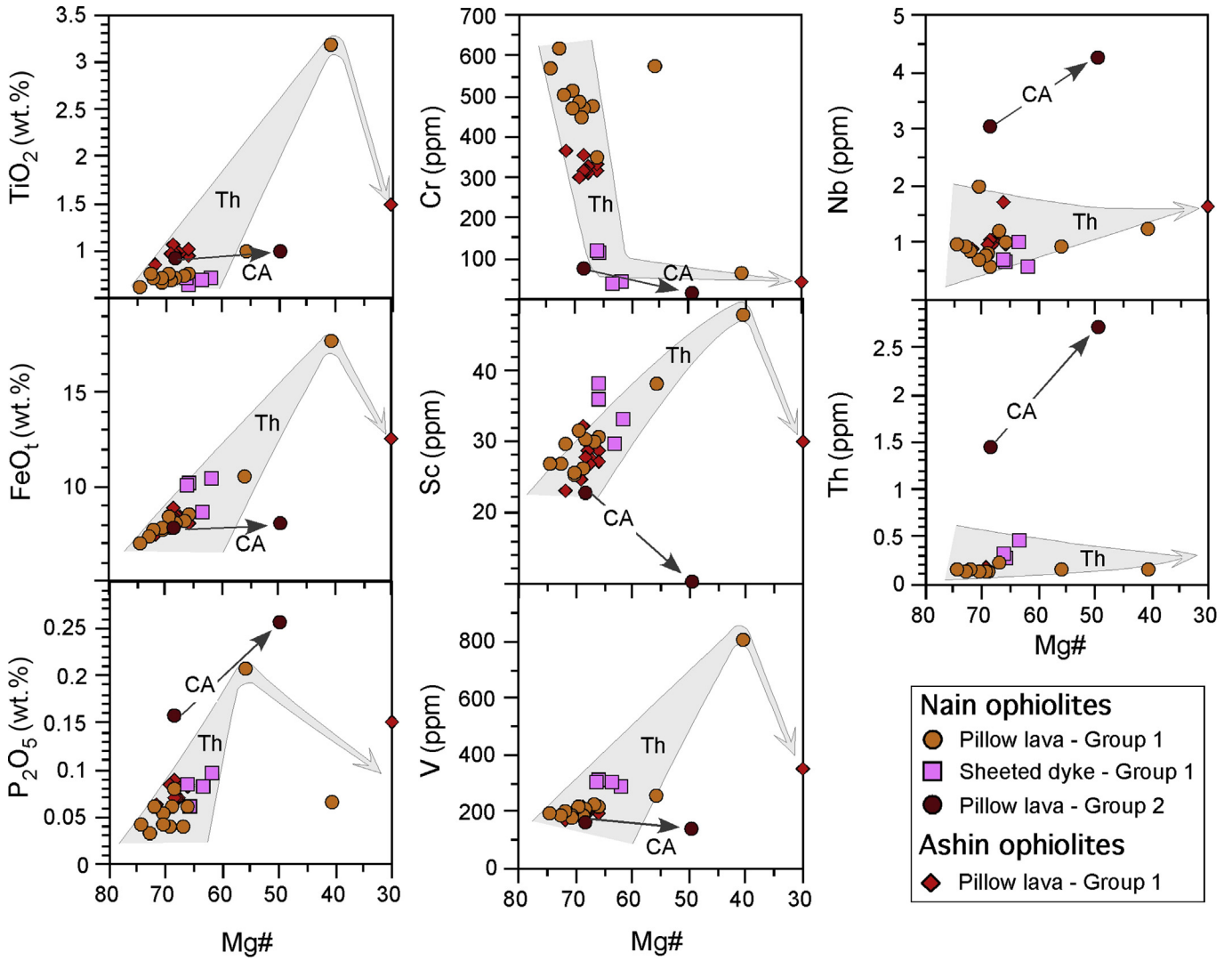

Figure 6. Variation in selected major and trace elements vs. Mg# [= MgO/(MgO + FeO)] for basaltic pillow lavas and sheeted dykes of the Nain and Ashin ophiolites. Major element oxides are recalculated on anhydrous bases. Arrows indicate general fractionation trends for the different rock-groups. Abbreviations, Th: Tholeiitic (Group 1); CA: calc-alkaline (Group 2).

Please cite this article as: Pirnia, T et al., Cretaceous tectonic evolution of the Neo-Tethys in Central Iran: Evidence from petrology and age of the Nain-Ashin ophiolitic basalts, Geoscience Frontiers, https://doi.org/10.1016/j.gsf.2019.02.008

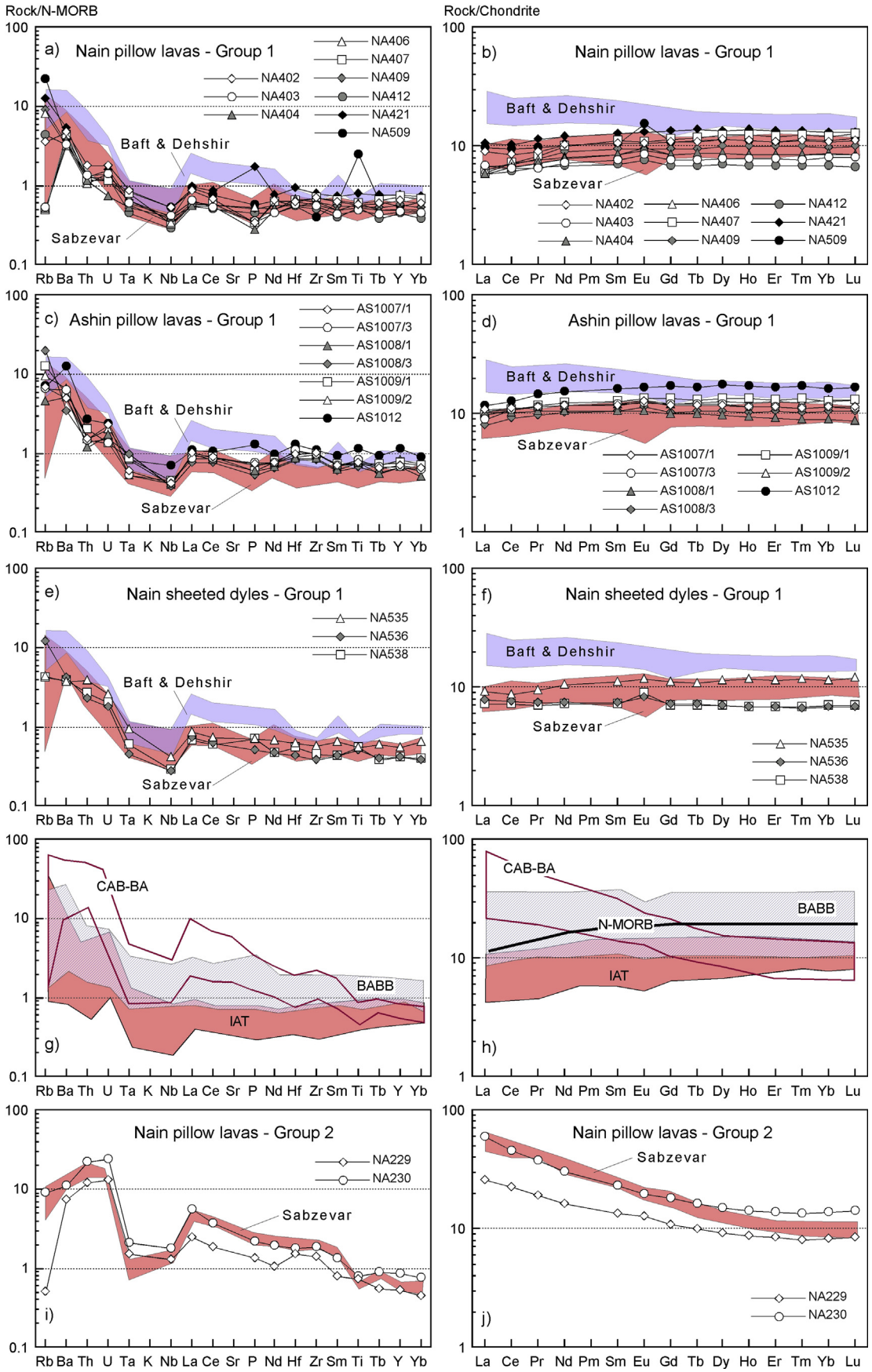

Please cite this article as: Pirnia, T et al., Cretaceous tectonic evolution of the Neo-Tethys in Central Iran: Evidence from petrology and age of the Nain-Ashin ophiolitic basalts, Geoscience Frontiers, https://doi.org/10.1016/j.gsf.2019.02.008

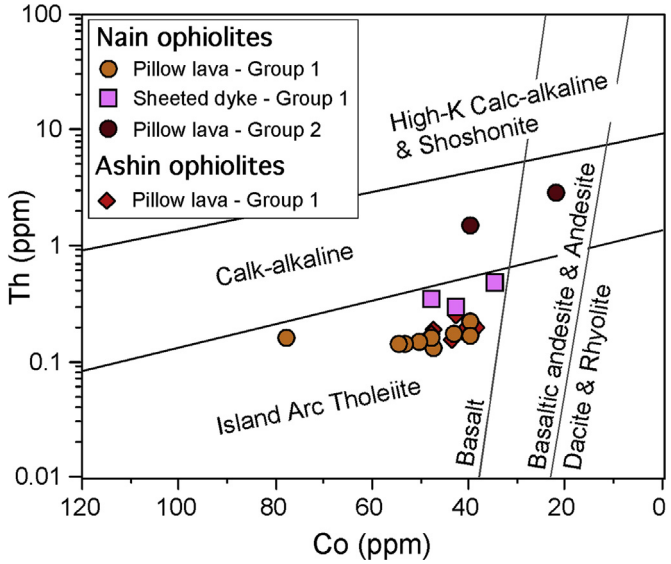

Figure 8. Th vs. Co discrimination diagram (Hastie et al., 2007) for basaltic pillow lavas and sheeted dykes of the Nain and Ashin ophiolites.

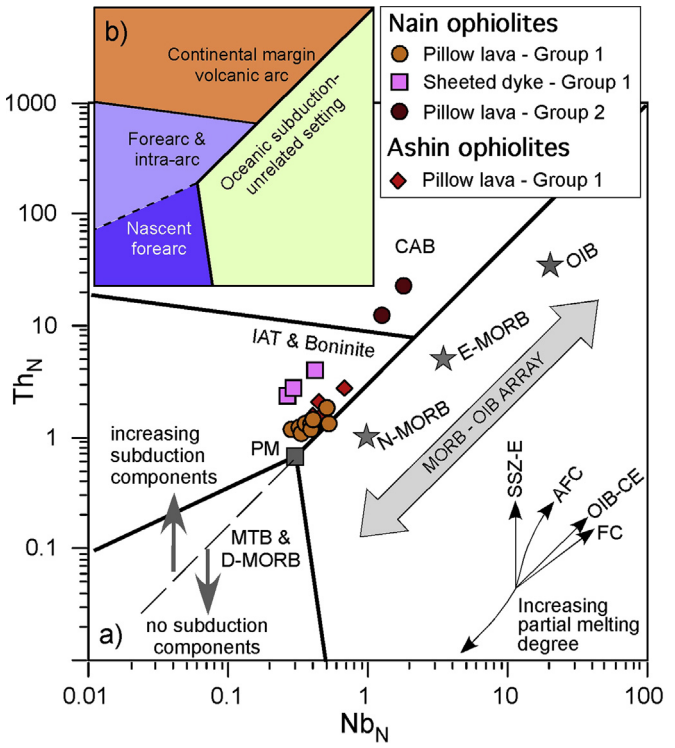

Figure 9. N-MORB-normalized Th vs. Nb discrimination diagram of Saccani (2015) for basaltic pillow lavas and sheeted dykes of the Nain and Ashin ophiolites. (a) Rock types, (b) tectonic setting interpretation. Abbreviations, MORB: mid-ocean ridge basalt, N-: normal type, E-: enriched type, D-: depleted type, MTB: medium Ti basalt; IAT: island arc tholeiite, CAB: calc-alkaline basalt; OIB: alkaline oceanic within-plate basalt; SSZ-E: supra-subduction zone enrichment; AFC: assimilation-fractional crystallization; OIB-CE: OIB component enrichment; FC: fractional crystallization. Normalization values, as well as the composition of typical N-MORB, EMORB, and OIB (stars) are from Sun and McDonough (1989).

overlying radiolarian cherts are mainly transitional. Interpillow patches of radiolarian chert are common (Fig. 2f). The thickness of radiolarian chert sequences range is about 25 m. The sampled radiolarian cherts AS1010, AS1012/1, and AS1021 were stratigraphically associated with pillow lava sample AS1012.

3. Radiolarian biostratigraphy

The radiolarian samples were etched with hydrochloric and hydrofluoric acid following the method proposed by Dumitrica (1970), Pessagno and Newport (1972), Baumgartner et al. (1981) and De Wever (1982). Unfortunately, some of them were barren or yielded radiolarians with very poor preservation. Three samples were however suitable for biostratigraphical analysis, thought two samples from the Nain ophiolite yielded radiolarians with moderate preservation. The principal marker taxa are illustrated in Fig. 3. From the analyzed cherts radiolarian assemblages and ages were obtained as follows.

Sample AS1010 contains a moderately well-preserved radiolarian assemblage dominated by nassellarians. All identified species are illustrated in Fig. 3. Age determination is primarily based on the zonation proposed by O'Dogherty (1994) and we mostly followed his systematics for determination of species. The names of genera are updated according to more recent publications (O'Dogherty et al., 2009, 2017).

The sample is assignable to UA 10 of the Romanus Subzone, the lower subzone of the Spoletoensis Zone. This assignment is constrained with the first occurrence of *Mita gracilis* (Squinabol) and the last occurrence of *Crococapsa asseni* (Tan). The Romanus Subzone is calibrated to the Middle Albian but we also note that the Early to early Middle Albian is not recorded in this zonation (see Figs. 10c and 11 in O'Dogherty, 1994). The first occurrence of *M. gracilis* (Squinabol) was later determined at the base of the Albian (Danelian, 2008). Based on these ranges, the inferred age for sample 1010 is Early–Middle Albian.

Samples NA424 and NA510 contain very few radiolarians determinable only at genus level. Both samples contain the genus *Dictyomitra*, which first appears in the Berriasian (O'Dogherty et al., 2009). The samples indicate the Cretaceous but a more precise age assignment is not possible.

4. Petrography of the sheeted dykes and pillow lavas

Most of the rocks studied in this paper are affected by various degrees of low-grade ocean-floor hydrothermal alteration, which resulted in different extent of replacement of the primary igneous phases. However, regardless of the extent of mineralogical alteration, the primary igneous textures are always well preserved. Olivine is never preserved, and it is always replaced by iddingsite and/or chlorite. Fresh plagioclase is very rare, since it is usually replaced by albite and calcite. Clinopyroxene alteration normally occurs as pseudomorphic replacement by chlorite or actinolitic amphibole; however, some samples display fresh clinopyroxene

Figure 7. N-MORB normalized incompatible element patterns (a, c, e, g, i) and chondrite-normalized REE patterns (b, d, f, h, j) for basaltic pillow lavas and sheeted dykes of the Nain and Ashin ophiolites. The compositions of basaltic pillow lavas and dykes from the Baft and Dehshir (Shafaii Moghadam et al., 2009), and Sabzevar (Rezaei et al., 2018) ophiolites are also shown. The compositions of island arc tholeiites (IAT), calc-alkaline basalts and basaltic andesites (CAB-BA), and backarc basin basalts (BABB) from various ophiolitic complexes and modern oceanic settings, as well as modern normal-type mid-ocean ridge basalt (N-MORB) are shown for comparison in panels (g) and (h). Data source, IAT: Ewart et al. (1994); Yuan et al. (2005); Saccani et al. (2008a); CAB-BA: Ewart et al. (1994); Saccani et al. (2008b); BABB: Ewart et al. (1994); Yuan et al. (2005); Saccani et al. (2008b); Rolland et al. (2009). Normalizing values and the compositions of N-MORB are from Sun and McDonough (1989).

Please cite this article as: Pirnia, T et al., Cretaceous tectonic evolution of the Neo-Tethys in Central Iran: Evidence from petrology and age of the Nain-Ashin ophiolitic basalts, Geoscience Frontiers, https://doi.org/10.1016/j.gsf.2019.02.008

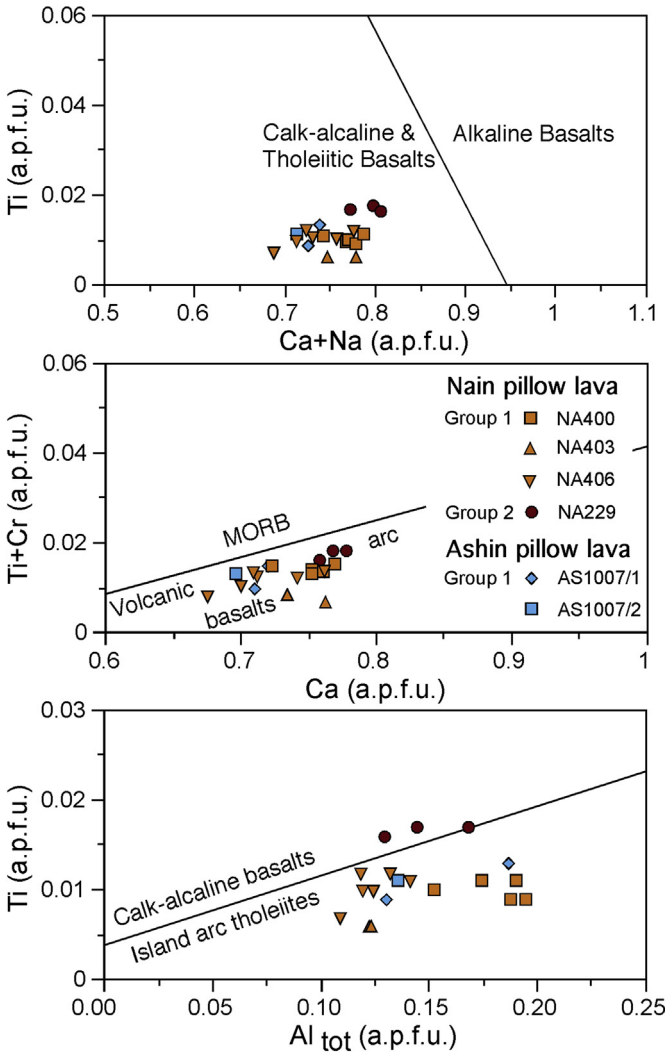

Figure 10. (a) Ti vs. (Ca + Na), (b) (Ti + Cr) vs. Ca, and (c) Ti vs. Al_{tot} discrimination diagrams of Leterrier et al. (1982) showing the composition of clinopyroxenes from the Group 1 (island arc tholeiite) and Group 2 (calc-alkaline) pillow lavas from the Nain and Ashin ophiolites.

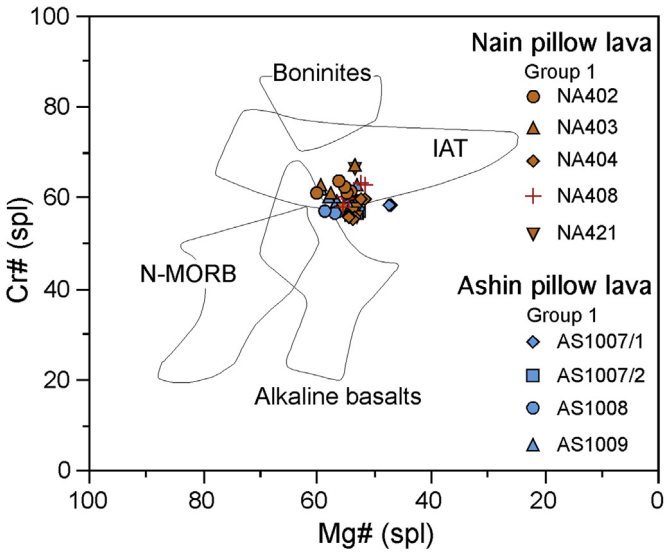

Figure 11. Mg# vs. Cr# diagram for spinels (spl) from the Group 1 (island arc tholeiite) pillow lavas from the Nain and Ashin ophiolites. Mg# = $Mg/(Mg + Fe^{2+})$, Cr# = Cr/(Cr + Al). The compositional variations of chromian spinels from alkaline basalts, boninites, island arc tholeiites (IAT), and normal-type mid-ocean ridge basalt (N-MORB) are also shown. Data from Hébert et al. (2003) and references therein.

relics as both phenocrysts and groundmass minerals. Volcanic glass in the groundmass has been altered into an assemblage of chlorite and prehnite. Few samples exhibit variolitic textures, with varioles filled by calcite and, subordinately, by chlorite and zeolite. In addition, small calcite veins are frequent. Regardless of the secondary mineralogical transformations, the following petrographic description will be made on the basis of the primary igneous phases.

4.1. Nain pillow lavas

Samples from NA400 to NA421 are olivine-basalt in composition, whereas sample NA509 is represented by a ferrobasalt. All these rocks belong to the geochemical Group 1, as will be defined in Section 6.2. Olivine-basalts show porphyritic, hypoialine textures with phenocrysts and microphenocrysts mainly represented by olivine (Fig. 4a) and plagioclase. Some samples display glomeroporphyritic texture with clusters made up of 3–4 plagioclase phenocrysts. Olivines form euhedral crystals, which often contain inclusions of glass (completely altered) and/or chromian spinel. Plagioclase phenocrysts commonly show albite-carlsbad twinning. The groundmass mainly shows hypoialine, intersertal textures with plagioclase laths and intergranular clinopyroxene, glass, and minor opaque minerals (Fig. 4a). In samples NA229 and NA230 (i.e. the samples belonging to the geochemical Group 2, as defined in Section 6.3) olivine is absent and the phenocryst assemblage is composed of plagioclase and plagioclase + clinopyroxene, respectively (Fig. 4b). In all samples, the groundmass shows intersertal and subophitic texture with plagioclase, clinopyroxene, altered glass, chromian spinel, and minor opaque minerals. The chromian spinels often contain inclusions of altered silicate minerals. The groundmass of sample NA230 shows fluidal texture marked by the alignment of plagioclase laths.

4.2. Nain sheeted dykes

Nain sheeted dykes are basalt and basaltic andesite in composition. They show intergranular texture and are mainly composed of plagioclase, altered clinopyroxene and hornblende (Fig. 4c). Minor amounts of quartz, Fe-Ti oxides and sulfides are in interstitial position between the major rock-forming minerals. Small apatite crystals occasionally occur as inclusions within plagioclases.

4.3. Ashin pillow lavas

Ashin pillow lavas range in composition from olivine-basalt to basaltic andesite. They show porphyritic to vitrophyric textures similar to those of the Nain pillow lavas. Phenocrysts and microphenocrysts are mainly represented by olivine, plagioclase, and clinopyroxene. The groundmass is intergranular, hypoialine in texture and is composed of plagioclase laths, granular clinopyroxene, altered glass, chromian spinel, and Fe-Ti oxides. Locally, the groundmass also includes sulfide minerals. Samples AS1007/2 and AS1008 also include minor amounts of primary hornblende as microphenocrysts. The chromian spinel is commonly represented by coarse-grained, euhedral crystals with inclusions of silicate minerals (Fig. 4d).

Please cite this article as: Pirnia, T et al., Cretaceous tectonic evolution of the Neo-Tethys in Central Iran: Evidence from petrology and age of the Nain-Ashin ophiolitic basalts, Geoscience Frontiers, https://doi.org/10.1016/j.gsf.2019.02.008

5. Analytical methods

Whole-rock major and some trace elements were analyzed by X-ray fluorescence (XRF) on pressed-powder pellets, using an ARL Advant-XP automated X-ray spectrometer. The matrix correction methods proposed by Lachance and Traill (1966) were applied. Volatile contents were determined as loss on ignition (L.O.I.) at 1000 °C. In addition, Rb, Sr, Zr, Y, Nb, Hf, Ta, Th, U, and the rare earth elements (REE) were determined by inductively coupled plasma-mass spectrometry (ICP-MS) using a Thermo Series X-I spectrometer. The results are shown in Table 1. However, for the discussion of the geochemical characteristics major element composition has been re-calculated on L.O.I.-free bases. The accuracy of the data for XRF and ICP-MS analyses were evaluated using results for international standard rocks run as unknown. The detection limits for XRF and ICP-MS analyses were evaluated using results from several runs of twenty-nine international standards. Results are given in Supplementary Table 1. All whole-rock analyses were performed at the Department of Physics and Earth Science, University of Ferrara.

Major element compositions of mineral phases were determined by electron microprobe spectrometry using a JEOL JXA8200 Superprobe at Leoben University, Austria. An accelerating voltage of 15 kV and a beam current of 10 nA were applied for 25 s counting interval, whereas the beam spot size was ~5 μm. The obtained major element results, corrected by an on-line ZAF program, are shown in Tables 2 and 3, Supplementary Table 1.

6. Whole rock chemistry of sheeted dykes and pillow lavas

6.1. Evaluation of the alteration effects

The geochemical features of the Nain and Ashin pillow lavas and dykes are described using basically those elements that are virtually immobile during low-temperature alteration and metamorphism. They include some incompatible trace elements (e.g., Ti, P, Zr, Y, Sc, Nb, Ta, Hf, Th), middle REE (M-REE) and heavy REE (H-REE), as well as some transition metals (e.g., Ni, Co, Cr, V). Large ion lithophile elements (LILE) and many major elements are commonly mobilized during alteration (e.g., Pearce and Norry, 1979). In addition, light REE (LREE) may also be affected to some degree of mobilization induced by alteration (e.g., Valsami and Cann, 1992). Some mobility tests were therefore made for SiO_2, Al_2O_3, FeO, CaO, Na_2O, K_2O, Ba, Rb, Sr, Pb, U, La, and Ce by plotting these elements versus some immobile elements (e.g., Zr, Y) and then by calculating the correlation coefficients (r^2) for samples from the different rock-types. These tests indicate that La (e.g., r^2 vs. Zr = 0.73–0.93), Ce (e.g., r^2 vs. Y = 0.82–0.99), and Ba (e.g., r^2 vs. Y = 0.67–0.88) show good correlation with immobile elements suggesting that the amount of mobilization of these elements was limited. Al_2O_3 (r^2 vs. Y = 0.55–0.72) resulted moderately mobilized in all the studied samples. In consequence, this element can be used, thought with some caution. Tests on SiO_2, FeO, CaO, Na_2O, and U returned different results depending on the rock-type. SiO_2, Na_2O, and U were little mobilized in samples from the Ashin pillow lavas and Nain sheeted dykes (r^2 vs. Y > 0.75, >0.80, and >0.72 for SiO_2, Na_2O, and U, respectively), whereas these elements were mobilized in samples from the Nain pillow lavas (r^2 vs. Y = 0.28, 0.45, and 0.11, respectively). FeO and CaO contents show good correlation with immobile elements for pillow lava samples from both the Nain and Ashin (e.g., r^2 for FeO vs. Y = 0.77–0.92 and r^2 for CaO vs. Y = 0.75–0.82). In contrast, these elements resulted fairly mobilized in samples from the Nain sheeted dykes (e.g., r^2 for FeO vs. Y = 0.24 and r^2 for CaO vs. Y = 0.48). K_2O (r^2 vs. Y < 0.48), Rb (r^2 vs. Y < 0.23), Pb (r^2 vs. Y < 0.36), and Sr (r^2 vs. Y < 0.22) contents resulted affected by high degrees of alteration-induced mobilization and therefore these elements cannot be used. The results obtained from the mobility tests carried out on the studied rocks are in agreement with previous works, which show that alteration of arc lithosphere by seawater or hydrothermal fluids increases the content of volatiles and trace elements, such as K, Rb, U, Pb, and Sr (e.g., Kelley et al., 2003).

6.2. Group 1 basaltic rocks

Group 1 rocks is represented by pillow lavas from both Nain and Ashin ophiolites, as well as by the Nain sheeted dykes. Group 1 pillow lavas from both Nain and Ashin pillow lava series show similar compositions and therefore they will be treated together in the following description. They are mainly represented by basalts, though one sample (NA509) showing ferrobasaltic composition and one sample (AS1012) showing basaltic andesitic composition are found in the pillow lava series of the Nain and Ashin ophiolites, respectively (Table 1). In basalts, SiO_2 contents range between 45.88 and 50.94 wt.% and Mg# range between 74.5 and 55.9, whereas in the ferrobasalt Mg# is low (40.7). The basaltic andesite shows comparatively higher fractionation degree with SiO_2 = 54.39 wt.% and Mg# = 30.1. These rocks display a sub-alkaline, tholeiitic nature exemplified by generally low Nb/Y ratios (Fig. 5), as well as by sharp Ti, Fe, P_2O_5, Sc, and V increase from basalt to ferrobasalt followed by a significant decrease in the basaltic andesite (Fig. 6). Basalts are characterized by variable, but generally low TiO_2 (0.60–1.05 wt.%), P_2O_5 (0.03–0.20 wt%), Zr (37–78 ppm) and Y (13–24 ppm) contents. Compatible element contents are very variable (e.g., Cr = 352–619 ppm). Nonetheless, these elements generally show high contents in most samples (Table 3). The ferrobasaltic sample obviously show very high FeO_t (17.74 wt.%), TiO_2 (3.06 wt.%), and V (807 ppm) contents. Normal-type MORB (N-MORB) normalized spiderdiagrams (Fig. 7a, c) display incompatible element patterns with a slight Th relative enrichment and marked Ta and Nb negative anomalies. High-field-strength element (HFSE) abundance is generally low ranging from 0.3 to 3 times N-MORB composition (Sun and McDonough, 1989). Most samples show REE patterns slightly increasing from LREE to HREE, whereas a few samples show almost flat patterns (Fig. 7b, d) as testified by the $(La/Sm)_N$ and $(La/Yb)_N$ ratios (0.54–0.98 and 0.50–1.14, respectively).

Group 1 rocks from the sheeted dykes of the Nain ophiolites show chemical features that are similar to those of Group 1 pillow lavas, though some minor differences can be observed. They are represented by basalts and basaltic andesites (Table 1), with SiO_2 contents ranging between 50.55 and 52.61 wt.%. Similar to pillow lava samples, these rocks display a sub-alkaline nature with low Nb/Y ratios (Fig. 5). They show uniform chemical composition (Table 1), as exemplified by the quite restricted range of variation of the Mg# values (66.2–61.9). Group 1 sheeted dykes are characterized by low TiO_2 (0.63–0.69 wt.%), P_2O_5 (0.06–0.09 wt.%), Zr (27–39 ppm), and Y (12–15 ppm) contents. Compatible element contents are generally low (e.g., Cr = 38–117 ppm) and comparatively lower, at comparable MgO contents, with respect to those observed in pillow lavas (Table 1). N-MORB normalized spiderdiagrams display incompatible element patterns with a slight Th relative enrichment and Ta and Nb negative anomalies (Fig. 7e). In particular, the Th relative enrichment (Th_N = 2.35–3.90) is higher compared to that of Group 1 pillow lava basaltic rocks (Th_N = 1.06–2.03). HFSE abundance is generally low ranging from 0.3 to 0.9 times N-MORB composition (Sun and McDonough, 1989). Chondrite-normalized REE abundance show either patterns slightly depleted in LREE compared to HREE ($(La/Yb)_N$ = 0.80) or slightly enriched in LREE compared to HREE ($(La/Yb)_N$ = 1.14) (Fig. 7f).

Please cite this article as: Pirnia, T et al., Cretaceous tectonic evolution of the Neo-Tethys in Central Iran: Evidence from petrology and age of the Nain-Ashin ophiolitic basalts, Geoscience Frontiers, https://doi.org/10.1016/j.gsf.2019.02.008

Table 1
Major oxides (wt.%) and trace element (ppm) analyses of pillow lavas and sheeted dykes of the Nain and Ashin ophiolites.

	Nain ophiolites									
	Group 1 (IAT) pillow lavas									
Latitude	33°09′36.5″	33°09′36.5″	33°09′36.5″	33°09′36.5″	33°09′36.5″	33°09′36.5″	33°09′36.5″	33°09′36.5″	33°09′36.5″	33°09′36.5″
Longitude	53°00′8.02″	53°00′8.02″	53°00′8.02″	53°00′8.02″	53°00′8.02″	53°00′8.02″	53°00′8.02″	53°00′8.02″	53°00′8.02″	53°00′8.02″
Sample	NA400	NA402	NA403	NA404	NA405	NA406	NA407	NA408	NA409	NA412
Rock	basalt	basalt	basalt	basalt	basalt	basalt	basalt	basalt	basalt	basalt
XRF Analyses:										
SiO_2	47.81	49.19	47.41	50.94	47.84	47.04	49.68	48.37	48.96	45.88
TiO_2	0.73	0.73	0.60	0.75	0.68	0.65	0.76	0.69	0.70	0.64
Al_2O_3	14.26	13.74	12.61	13.92	12.40	14.00	14.69	13.31	14.77	13.25
Fe_2O_3	1.09	1.05	0.88	0.94	0.99	0.99	1.11	1.03	0.99	0.96
FeO	7.29	7.03	5.89	6.27	6.60	6.60	7.38	6.88	6.63	6.40
MnO	0.15	0.15	0.14	0.14	0.13	0.14	0.15	0.14	0.14	0.13
MgO	7.93	7.94	9.65	9.41	8.88	8.20	9.41	8.33	9.59	8.59
CaO	13.36	14.39	15.97	12.13	14.76	13.18	12.86	13.07	11.79	15.16
Na_2O	3.31	2.87	2.28	2.32	2.97	3.50	3.10	3.64	3.25	3.15
K_2O	0.50	0.11	0.03	0.01	b.d.l.	0.56	0.00	0.61	0.54	0.54
P_2O_5	0.06	0.04	0.04	0.03	0.04	0.06	0.04	0.08	0.06	0.05
L.O.I.	4.07	3.56	5.28	2.32	5.16	5.32	1.35	4.60	2.99	4.80
Total	100.56	100.78	100.78	99.19	100.44	100.24	100.52	100.74	100.41	99.56
Mg#	66.0	66.8	74.5	72.8	70.5	68.9	69.5	68.3	72.0	70.5
Zn	64	67	53	57	60	58	72	62	65	55
Cu	53	79	76	80	80	35	82	77	80	80
Sc	31	30	27	27	26	26	31	30	30	25
Ga	12	13	12	12	12	12	13	11	11	12
Ni	69	136	192	220	199	105	169	91	133	134
Co	42	40	43	53	46	47	50	42	48	55
Cr	352	479	570	619	516	451	485	470	504	471
V	218	226	197	185	177	186	219	213	202	188
Ba	27	30	21.4	24	20	20	28	25	22	21
Pb	10	9	9	8	10	7	7	8	10	8
ICP-MS Analyses (**indicates values obtained by XRF analyses*):										
Rb	4*	2.06	0.305	0.286	5*	4.61	0.280	6*	5.19	2.50
Sr	200*	150	119	112	128*	161	113	183*	154	144
Y	17*	18.6	13.3	14.2	14*	14.0	20.5	15*	16.0	12.6
Zr	49*	51.4	40.3	48.1	45*	41.0	52.7	41*	44.7	36.7
La	b.d.l.*	2.17	1.64	1.37	b.d.l.*	1.50	1.44	b.d.l.*	1.59	1.40
Ce	b.d.l.*	5.23	4.03	4.13	b.d.l.*	4.40	4.45	b.d.l.*	4.35	3.81
Pr		0.862	0.621	0.688		0.724	0.798		0.741	0.640
Nd	4*	4.81	3.37	3.71	b.d.l.*	3.75	4.67	5*	4.17	3.26
Sm		1.64	1.17	1.31		1.29	1.72		1.47	1.08
Eu		0.625	0.491	0.574		0.534	0.638		0.554	0.447
Gd		2.24	1.57	1.78		1.75	2.35		1.96	1.41
Tb		0.412	0.290	0.325		0.326	0.448		0.360	0.261
Dy		2.90	2.00	2.23		2.24	3.18		2.56	1.79
Ho		0.644	0.442	0.484		0.484	0.716		0.574	0.391
Er		1.83	1.30	1.42		1.43	2.03		1.66	1.15
Tm		0.288	0.198	0.217		0.216	0.318		0.260	0.175
Yb		1.87	1.36	1.48		1.46	2.09		1.65	1.18
Lu		0.288	0.204	0.219		0.217	0.322		0.255	0.172
Nb	1*	1.23	0.977	0.946	1*	0.801	0.772	1*	0.854	0.689
Hf		1.30	1.18	1.41		1.31	1.35		1.14	1.13
Ta		0.116	0.080	0.069		0.077	0.105		0.086	0.061
Th	b.d.l.*	0.219	0.167	0.140	b.d.l.*	0.128	0.145	b.d.l.*	0.157	0.137
U		0.085	0.068	0.035		0.071	0.054		0.054	0.059
Ti/V	21	20	19	25	24	22	21	20	21	22
Nb/Y	0.06	0.07	0.07	0.07	0.07	0.06	0.04	0.04	0.05	0.05
$(La/Sm)_N$		0.85	0.90	0.67		0.75	0.54		0.70	0.84
$(Sm/Yb)_N$		0.98	0.95	0.98		0.98	0.91		0.99	1.02
$(La/Yb)_N$		0.83	0.86	0.66		0.74	0.50		0.69	0.85

	Nain ophiolites							
	Group 1 (IAT) pillow lavas		Group 2 (CAB) pillow lavas		Group 1 (IAT) sheeted dyke			
Latitude	33°09′19.2″	33°09′54.9″	33°09′5.6″	33°09′5.6″	33°09′02.7″	33°09′02.7″	33°09′02.7″	33°09′02.7″
Longitude	53°00′40.8″	53°01′00.0″	53°00′36.4″	53°00′36.4″	53°01′55.5″	53°01′55.5″	53°01′55.5″	53°01′55.5″
Sample	NA421	NA509	NA229	NA230	NA535	NA536	NA537	NA538
Rock	basalt	Fe-basalt	basalt	basalt	basalt	basalt	bas and	basalt
XRF Analyses:								
SiO_2	50.89	45.39	50.81	51.53	52.09	51.20	52.61	50.55
TiO_2	0.98	3.06	0.90	0.96	0.69	0.63	0.69	0.69
Al_2O_3	13.89	15.72	16.26	15.32	11.62	14.37	13.48	14.08
Fe_2O_3	1.36	2.25	0.99	1.01	1.12	1.31	1.34	1.29
FeO	9.09	15.03	6.63	6.73	7.46	8.75	8.91	8.62
MnO	0.15	0.17	0.14	0.11	0.17	0.20	0.17	0.20

Please cite this article as: Pirnia, T et al., Cretaceous tectonic evolution of the Neo-Tethys in Central Iran: Evidence from petrology and age of the Nain-Ashin ophiolitic basalts, Geoscience Frontiers, https://doi.org/10.1016/j.gsf.2019.02.008

Table 1 (*continued*)

	Nain ophiolites							
	Group 1 (IAT) pillow lavas		Group 2 (CAB) pillow lavas		Group 1 (IAT) sheeted dyke			
MgO	6.48	5.78	8.07	3.72	7.27	9.49	8.12	9.47
CaO	8.75	5.03	7.12	8.38	12.42	7.11	6.79	8.03
Na_2O	5.07	3.29	5.05	6.76	4.47	3.29	4.20	3.78
K_2O	0.72	0.50	0.02	0.28	0.14	0.98	0.38	0.40
P_2O_5	0.20	0.06	0.15	0.24	0.08	0.06	0.09	0.08
LOI	3.40	2.96	4.29	4.77	2.59	2.76	2.35	2.69
Total	100.99	99.26	100.44	99.80	100.12	100.15	99.12	99.89
Mg#	55.9	40.7	68.4	49.6	63.5	65.9	61.9	66.2
Zn	189	212	76	68	28	42	49	40
Cu	24	27	106	24	106	50	32	13
Sc	38	48	23	10	30	38	33	36
Ga	12	21	16	20	15	14	13	13
Ni	41	39	12	b.d.l.	13	23	12	22
Co	40	78	40	22	35	43	47	48
Cr	574	68	77	17	38	114	41	117
V	258	807	166	137	306	308	292	303
Ba	34	25	47	71	24	27	24	25
Pb	10	7	14	21	10	7	7	10
ICP-MS Analyses (**indicates values obtained by XRF analyses*):								
Rb	7.07	12.7	0.289	5.06	2.48	6.71	3*	2.42
Sr	203	253	190	577	109	125	133*	71
Y	21.6	15.8	14.7	24.6	15.5	11.8	15*	11.6
Zr	65.7	33.1	107	136	35.7	27.3	39*	31.5
La	2.51	2.35	6.24	14.15	2.20	1.88	b.d.l.*	1.73
Ce	6.42	5.81	13.87	27.9	5.46	4.65	b.d.l.*	4.48
Pr	1.09	0.920	1.83	3.57	0.908	0.708		0.679
Nd	5.73	4.86	7.70	14.4	5.01	3.52	4*	3.41
Sm	1.95	1.63	2.10	3.58	1.73	1.15		1.13
Eu	0.765	0.896	0.742	1.16	0.681	0.488		0.525
Gd	2.82	2.25	2.23	3.72	2.29	1.50		1.47
Tb	0.523	0.415	0.376	0.608	0.412	0.270		0.264
Dy	3.46	2.93	2.38	3.84	2.94	1.82		1.81
Ho	0.782	0.641	0.504	0.812	0.665	0.393		0.390
Er	2.26	1.82	1.42	2.33	1.91	1.15		1.15
Tm	0.346	0.292	0.209	0.347	0.304	0.173		0.176
Yb	2.26	1.90	1.40	2.34	1.97	1.18		1.21
Lu	0.339	0.298	0.216	0.362	0.309	0.176		0.181
Nb	0.940	1.26	3.05	4.27	0.994	0.645	1*	0.691
Hf	1.97	1.16	3.129	3.709	1.288	0.908		1.148
Ta	0.088	0.109	0.203	0.276	0.126	0.061		0.079
Th	0.159	0.155	1.45	2.72	0.467	0.282	b.d.l.*	0.330
U	0.076	0.060	0.611	1.16	0.123	0.084		0.097
Ti/V	23	24	34	44	14	13	15	14
Nb/Y	0.04	0.08	0.21	0.17	0.06	0.05	0.04	0.06
$(La/Sm)_N$	0.83	0.93	1.92	2.55	0.82	1.06		0.99
$(Sm/Yb)_N$	0.96	0.95	1.66	1.70	0.98	1.08		1.03
$(La/Yb)_N$	0.80	0.88	3.19	4.33	0.80	1.14		1.02

	Ashin ophiolites									
	Group 1 (IAT) pillow lavas									
Latitude	33°31′33.3″	33°31′33.3″	33°31′06.4″	33°31′33.3″	33°31′37.7″	33°31′33.3″	33°31′43.2″	33°31′33.3″	33°31′33.3″	33°31′47.4″
Longitude	53°23′52.8″	53°23′52.8″	53°23′56.0″	53°23′52.8″	53°23′52.7″	53°23′52.8″	53°23′48.9″	53°23′52.8″	53°23′52.8″	53°23′48.4″
Sample	AS1007/1	AS1007/2	AS1007/3	AS1007/4	AS1008/1	AS1008/2	AS1008/3	AS1009/1	AS1009/2	AS1012
Rock	basalt	basalt	basalt	basalt	basalt	basalt	basalt	basalt	basalt	bas and
XRF Analyses:										
SiO_2	46.57	47.68	49.42	47.22	48.55	48.96	47.32	48.54	46.83	54.39
TiO_2	0.94	0.98	1.05	0.96	0.95	0.94	0.81	0.95	0.91	1.48
Al_2O_3	15.41	15.63	14.39	15.40	15.34	15.29	15.51	15.74	13.67	14.37
Fe_2O_3	1.07	1.09	1.15	1.08	1.06	1.06	0.95	1.09	1.03	1.65
FeO	7.12	7.26	7.68	7.18	7.08	7.03	6.33	7.26	6.86	10.99
MnO	0.13	0.17	0.14	0.14	0.14	0.14	0.13	0.12	0.13	0.17
MgO	8.94	7.93	9.43	8.48	8.51	8.60	9.04	8.48	7.47	2.66
CaO	11.85	10.94	9.70	12.26	11.64	11.46	11.85	11.05	14.47	5.82
Na_2O	3.29	3.59	4.02	3.42	3.65	3.75	3.25	3.55	4.01	7.24
K_2O	0.33	0.71	0.32	0.31	0.28	0.27	0.59	0.44	0.26	0.28
P_2O_5	0.08	0.08	0.09	0.08	0.07	0.07	0.06	0.07	0.08	0.15
LOI	3.85	3.31	2.72	3.82	2.96	3.13	3.94	3.29	5.22	0.85
Total	99.57	99.36	100.11	100.35	100.24	100.70	99.79	100.58	100.94	100.05
Mg#	69.1	66.0	68.6	67.8	68.2	68.5	71.8	67.6	66.0	30.1
Zn	64	67	75	66	68	65	54	67	70	108
Cu	64	66	71	68	71	71	69	70	68	22
Sc	25	27	32	27	29	28	23	28	29	30
Ga	14	14	12	14	13	13	13	14	14	11

(*continued on next page*)

Please cite this article as: Pirnia, T et al., Cretaceous tectonic evolution of the Neo-Tethys in Central Iran: Evidence from petrology and age of the Nain-Ashin ophiolitic basalts, Geoscience Frontiers, https://doi.org/10.1016/j.gsf.2019.02.008

Table 1 (*continued*)

	Ashin ophiolites									
	Group 1 (IAT) pillow lavas									
Ni	81	75	59	75	71	65	119	77	66	
Co	48	51	41	43	44	37	48	43	39	49
Cr	298	334	355	328	317	317	368	309	315	44
V	194	193	219	205	205	201	172	200	207	348
Ba	32	35.5	40	41	33	32	22	36	42	81
Pb	10	6	8	10	6	9	8	7	11	13
*ICP-MS Analyses (*indicates values obtained by XRF analyses)*:										
Rb	3.80	7*	3.70	2*	2.57	2*	11.2	7.11	5.39	4.10
Sr	297	211*	219	277*	222	244*	335	279	262	332
Y	19.7	20*	19.3	20*	19.0	18*	18.8	21.9	23.8	32.4
Zr	71.2	74*	78.2	71*	64.7	71*	59.8	73.0	66.7	87.1
La	2.59	b.d.l.*	2.15	b.d.l.*	2.48	b.d.l.*	1.92	2.34	2.52	2.80
Ce	6.91	8*	6.63	6*	6.40	6*	5.71	6.74	6.77	7.86
Pr	1.10		1.10		1.01		0.936	1.13	1.11	1.39
Nd	5.60	5*	5.61	6*	5.03	5*	4.80	5.83	5.61	7.32
Sm	1.84		1.87		1.63		1.61	1.96	1.88	2.49
Eu	0.738		0.722		0.621		0.661	0.779	0.764	0.975
Gd	2.42		2.47		2.08		2.13	2.79	2.50	3.57
Tb	0.439		0.454		0.376		0.396	0.489	0.470	0.639
Dy	3.00		3.07		2.51		2.72	3.46	3.24	4.49
Ho	0.650		0.659		0.536		0.590	0.767	0.718	0.987
Er	1.90		1.92		1.54		1.74	2.17	2.11	2.78
Tm	0.289		0.287		0.232		0.263	0.342	0.323	0.439
Yb	1.96		1.94		1.56		1.82	2.16	2.25	2.81
Lu	0.290		0.284		0.226		0.269	0.333	0.337	0.426
Nb	0.979	2*	1.06	1*	0.984	1*	0.911	1.08	0.955	1.65
Hf	2.06		2.26		1.81		1.70	2.148	1.880	2.719
Ta	0.080		0.071		0.070		0.131	0.113	0.110	0.112
Th	0.182	b.d.l.*	0.178	b.d.l.*	0.147	b.d.l.*	0.168	0.244	0.187	0.332
U	0.109		0.065		0.081		0.073	0.065	0.097	0.112
Ti/V	30	32	29	29	28	29	30	29	27	26
Nb/Y	0.05	0.09	0.06	0.05	0.05	0.08	0.05	0.05	0.04	0.05
$(La/Sm)_N$	0.91		0.74		0.98		0.77	0.77	0.87	0.73
$(Sm/Yb)_N$	1.04		1.07		1.16		0.98	1.01	0.93	0.99
$(La/Yb)_N$	0.95		0.80		1.14		0.76	0.78	0.80	0.71

Abbreviations, bas and: basaltic andesite; b.d.l.: below detection limit. Mg# = 100 × Mg/(Mg + Fe^{2+}). Fe_2O_3 is calculated assuming $Fe_2O_3 = 0.15 \times FeO$. Normalizing values for REE ratios are from Sun and McDonough (1989).

The overall geochemical features of Group 1 rocks from both Nain and Ashin pillow lavas and Nain sheeted dykes are similar to those of IAT from many ophiolitic complexes, as exemplified by the incompatible elements and REE concentrations (see Fig. 7g and h for a comparison). Based on Th-Co co-variation, Group 1 rocks can be classified as IAT (Fig. 8). Accordingly, in the discrimination diagrams of Fig. 9a they plot in the field for IAT rocks forming in volcanic arc settings with no significant contribution from polygenetic crust (Fig. 9b).

6.3. Group 2 basaltic rocks

Group 2 rocks include only a couple of samples from the Nain pillow lavas series. They are represented by basalts with SiO_2 contents ranging from 50.04 to 51.83 wt.%, whereas Mg# range from 68.4 to 49.6. These rocks display sub-alkaline nature as testified by low Nb/Y ratios (Fig. 5). Ti and Fe show a mild increase with decreasing Mg# (Fig. 6). Although generally low, TiO_2 (0.90–0.96 wt.%) and Y (15–25 ppm) contents are comparatively higher than those observed in Group 1 rocks. In contrast, P_2O_5 (0.15–0.24 wt.%) and Zr (107–136 ppm) contents are significantly higher than those of Group 1 rocks. Compatible element contents (Table 1) are very low (e.g., Ni < 12 ppm, Cr = 17–77 ppm). The incompatible element abundance (Fig. 7i) exhibits patterns, which are very similar to those of calc-alkaline (CA) basalts (e.g., Pearce, 1983) with marked positive anomalies in Th, U, La, and Ce, and negative anomalies in Ta, Nb, and Ti. The chondrite-normalized REE abundances (Fig. 7j) of the Group 2 pillow lavas have sub-parallel patterns, regularly decreasing from LREE to HREE. The enrichment in LREE compared to HREE is rather uniform with $(La/Yb)_N$ ratios ranging from 3.19 to 4.33. La generally varies from ~26 to ~60 times chondrite abundance. The incompatible elements and REE patterns (Fig. 7i and j) are consistent with a CA affinity for these rocks (see Fig. 7g and h for a comparison). In fact, Group 2 rocks plot in the field for CA basalts and basaltic andesites in the Th-Co diagram (Fig. 8). Accordingly, these samples plot in the field for CA basalts (Fig. 9a) formed at continental margin volcanic arc (Fig. 9b).

7. Mineral chemistry and geothermobarometry

Unfortunately, due to alteration effects, many of the studied samples were not suitable for electron microprobe analysis. In addition, in most of the analyzed samples, only one type of mineral phase was fresh enough to be analyzed, whereas only very few samples included two or three different types of fresh mineral phases. Nonetheless, we performed mineral chemistry analyses on a total of twelve samples for determining the compositions of clinopyroxene, Cr-spinel, plagioclase and amphibole. Most of the analyzed plagioclase showed, however, albite-oligoclase composition clearly reflecting a severe alteration of this mineral. Only in a couple of samples from the Nain pillow lava series (samples NA403 and NA404) few plagioclase crystals resulted relatively fresh, ranging in composition from labradorite to bytownite. However, the number of reliable plagioclase analyses is very limited and therefore this mineral will not be discussed in this work.

Please cite this article as: Pirnia, T et al., Cretaceous tectonic evolution of the Neo-Tethys in Central Iran: Evidence from petrology and age of the Nain-Ashin ophiolitic basalts, Geoscience Frontiers, https://doi.org/10.1016/j.gsf.2019.02.008

Table 2
Representative analyses of clinopyroxenes in Group 1 (island arc tholeiite) and Group 2 (calc-alkaline) pillow lavas from the Nain and Ashin ophiolites and estimated temperature (T, °C) and pressure (GPa) of crystallization.

Locality - unit	Nain ophiolites - pillow lavas											Ashin ophiolites - pillow lavas		
Rock group	Group 1 (island arc tholeiite)								Group 2 (calc-alkaline)			Group 1 (island arc tholeiite)		
Sample rock type	NA400 basalt			NA403 basalt		NA406 basalt			NA229 basalt			AS1007/1 basalt		AS1007/2 basalt
Mineral	cpx 1-19	cpx 3-22	cpx 10-28	cpx 5-1	cpx 5-2	cpx 4-3	cpx 8-10	cpx 9-11	cpx 1-1	cpx 1-2	cpx 8-10	cpx 10-20	cpx 11-21	cpx 1-1
Mineral type	Augite	Augite	Augite	Augite	Augite	Augite	Augite	Augite	Augite	Augite	Augite	Augite	Augite	Augite
SiO_2	51.31	51.00	51.17	52.25	53.78	53.06	52.77	52.84	52.30	52.06	51.56	51.29	53.26	51.90
TiO_2	0.40	0.35	0.34	0.21	0.22	0.27	0.44	0.37	0.63	0.58	0.61	0.48	0.32	0.41
Al_2O_3	4.02	3.49	4.49	2.88	2.90	2.58	3.11	2.90	3.35	3.00	3.93	4.37	3.03	3.13
Cr_2O_3	0.15	0.12	0.16	0.04	0.09	0.03	0.07	0.08	0.04	0.07	0.05	0.06	0.04	0.07
FeO	7.24	8.57	5.92	5.44	5.10	5.70	5.34	7.07	6.40	6.28	6.74	7.15	5.49	7.60
MnO	0.18	0.23	0.18	0.17	0.15	0.21	0.14	0.20	0.17	0.10	0.20	0.14	0.22	0.21
MgO	16.62	16.23	17.33	18.88	19.31	20.64	18.75	18.05	17.05	17.32	17.67	18.02	18.61	18.19
CaO	19.53	18.93	19.06	19.57	19.07	17.51	19.73	19.10	19.63	19.82	19.13	18.49	18.19	17.71
Na_2O	0.27	0.25	0.23	0.23	0.19	0.20	0.22	0.25	0.42	0.41	0.39	0.26	0.22	0.26
K_2O	0.00	0.00	0.00	0.00	0.01	0.00	0.00	0.00	0.00	0.00	0.00	0.00	0.00	0.00
Total	99.72	99.17	98.89	99.66	100.82	100.20	100.57	100.86	99.98	99.64	100.27	100.25	99.37	99.49
*Fe_2O_3	1.76	2.08	1.10	3.00	0.53	2.64	1.91	1.73	1.05	1.95	2.82	2.82	0.00	1.91
*FeO	5.65	6.70	4.93	2.74	4.62	3.33	3.62	5.51	5.45	4.53	4.20	4.61	5.49	5.88
*Total	99.89	99.38	99.00	99.96	100.87	100.46	100.77	101.03	100.09	99.84	100.56	100.54	99.37	99.68
a.p.f.u.														
Si	1.885	1.892	1.884	1.899	1.931	1.909	1.903	1.912	1.910	1.906	1.873	1.863	1.941	1.903
Ti	0.011	0.010	0.009	0.006	0.006	0.007	0.012	0.010	0.017	0.016	0.017	0.013	0.009	0.011
Al	0.174	0.153	0.195	0.123	0.123	0.109	0.132	0.124	0.144	0.129	0.168	0.187	0.130	0.135
Cr	0.004	0.004	0.005	0.001	0.003	0.001	0.002	0.002	0.001	0.002	0.002	0.002	0.001	0.002
Fe^{3+}	0.049	0.058	0.031	0.082	0.014	0.071	0.052	0.047	0.029	0.054	0.077	0.077	0.000	0.053
Fe^{2+}	0.174	0.208	0.152	0.083	0.139	0.100	0.109	0.167	0.166	0.139	0.128	0.140	0.167	0.180
Mn	0.006	0.007	0.006	0.005	0.004	0.006	0.004	0.006	0.005	0.003	0.006	0.004	0.007	0.007
Mg	0.910	0.898	0.951	1.023	1.033	1.107	1.008	0.974	0.928	0.945	0.957	0.976	1.011	0.994
Ca	0.768	0.752	0.752	0.762	0.734	0.675	0.762	0.740	0.768	0.777	0.745	0.720	0.710	0.696
Na	0.019	0.018	0.016	0.016	0.013	0.014	0.015	0.018	0.030	0.029	0.027	0.018	0.015	0.019
K	0.000	0.000	0.000	0.000	0.000	0.000	0.000	0.000	0.000	0.000	0.000	0.000	0.000	0.000
Total	4.000	4.000	4.000	4.000	4.000	4.000	4.000	4.000	4.000	4.000	4.000	4.000	3.992	4.000
Al (iv)	0.115	0.108	0.116	0.101	0.069	0.091	0.097	0.088	0.090	0.094	0.127	0.137	0.059	0.097
Al (vi)	0.059	0.045	0.079	0.022	0.053	0.018	0.035	0.036	0.055	0.035	0.042	0.050	0.071	0.038
Wo (%)	40.0	38.9	39.5	38.8	37.9	34.3	39.2	38.1	40.0	40.0	38.5	37.3	37.3	35.8
En (%)	47.4	46.4	50.0	52.0	53.5	56.3	51.8	50.0	48.3	48.6	49.5	50.5	53.1	51.2
Fs (%)	11.6	13.7	9.6	8.4	7.9	8.7	8.3	11.0	10.2	9.9	10.6	11.2	8.8	12.0
Acm (%)	1.0	0.9	0.9	0.8	0.7	0.7	0.8	0.9	1.6	1.5	1.4	0.9	0.8	1.0
Mg#	80.4	77.2	83.9	86.1	87.1	86.6	86.2	82.0	82.6	83.1	82.4	81.8	85.8	81.0
T (°C)*	1195 ± 3			1223 ± 7		1192 ± 5			1223 ± 6			1224 ± 8		1205
P (GPa)*	0.29 ± 0.06			0.29 ± 0.08		0.22 ± 0.05			0.61 ± 0.03			0.54 ± 0.01		0.52

Abbreviations, Wo: wollastonite; En: enstatite; Fs: ferrosilite; Acm: acmite. Major element oxides are in wt.%. Atoms per formula units (a.p.f.u.) were calculated based on six equivalent oxigens. Mg# = 100 × Mg/(Mg + Fe^{2+}). Fe^{3+} and Fe^{2+}, as well as Fe_2O_3 and FeO compositions were calculated from total measured FeO according to the stoichiometric criteria proposed by Droop (1987). Temperatures were estimated according to Putirka et al. (2003), whereas pressures were estimated according to Putirka (2008).

7.1. Clinopyroxene

Fresh primary clinopyroxenes crystals were found in samples of Group 1 and Group 2 pillow lavas from both Nain and Ashin ophiolites, whereas no fresh crystals were found in Group 1 rocks from the Nain sheeted dykes. Representative analyses of fresh clinopyroxene crystals are given in Table 2. Clinopyroxenes in Group 1 pillow lavas from both Nain and Ashin ophiolites show augitic composition, according to the classification of Morimoto (1989). No significant chemical differenced can be seen between clinopyroxenes from samples from the Nain and Ashin Group 1 pillow lavas and therefore these samples will be described together in the following discussion. Clinopyroxenes from Group 1 rocks are characterized by low TiO_2 (0.21–0.48 wt.%) and Na_2O (0.19–0.29 wt.%) contents, whereas Mg# are relatively high (77.2–87.1). Cr_2O_3 contents are rather low, ranging from 0.03 to 0.09 wt.% in most samples. However, comparatively higher values can be seen in sample NA400, where Cr_2O_3 content varies from 0.12 to 0.16 wt.%. The Ti/Al ratio is assumed to vary as a function of the Ti-Al substitution in pyroxene, which, in turn, is strongly controlled by the magma composition. Ti/Al ratios displayed by clinopyroxenes from Group 1 basalts are generally very low (0.05–0.10). In these minerals, no definite correlations between Mg# and Ti, Na and Al are observed. Only clinopyroxenes in sample NA403, which shows the highest whole rock Mg#, display the lowest Ti and Na contents when compared to other clinopyroxenes (Table 2). In contrast, Ti and Na contents are positively correlated in all samples.

Clinopyroxenes from Group 2 basalts from the Nain pillow lava series are augitic in composition (Morimoto, 1989). Compared to clinopyroxenes from Group 1 basalts, they show higher TiO_2 (0.46–0.61 wt.%) and Na_2O (0.36–0.42 wt.%) contents (see Table 2). Accordingly, their Ti/Al ratios are generally higher than those observed in clinopyroxenes from Group 1 rocks, ranging from 0.10 to 0.12. However, Mg# (82.4–84.0) and Cr_2O_3 contents (0.04–0.12 wt.%) show values perfectly overlapping those observed in clinopyroxenes from Group 1 rocks (Table 2). In contrast to what

Please cite this article as: Pirnia, T et al., Cretaceous tectonic evolution of the Neo-Tethys in Central Iran: Evidence from petrology and age of the Nain-Ashin ophiolitic basalts, Geoscience Frontiers, https://doi.org/10.1016/j.gsf.2019.02.008

Table 3
Representative analyses of amphiboles in Group 1 (island arc tholeiite) sheeted dykes from the Nain ophiolites and pillow lavas from the Ashin ophiolites. Pressures (P, GPa) of crystallization estimated according to different methods are also shown.

Locality - unit	Nain - sheeted dykes										Ashin - pillow lavas	
Sample rock type	NA537 basaltic andesite						NA538 basalt				AS1007/2 basalt	AS1008 basalt
Mineral	am 2-5c	am 2-5r	am 10-2c	am 10-2r	am 12-1c	am 12-1r	am 4-4c	am 4-4r	am 10-9c	am 10-9r	am 8-3c	am 7-11c
Mineral type	Mhb	Mhb	Mhb	Mhb	Mhb	Mhb	Mhb	Mhb	Mhb	Mhb	Mhb	Mhb
SiO_2	51.08	50.69	49.99	51.02	50.77	50.71	50.15	50.56	50.89	50.17	50.07	50.30
TiO_2	0.59	1.09	0.85	1.14	0.65	0.93	0.51	0.68	0.36	0.52	1.11	2.18
Al_2O_3	6.46	7.86	7.84	8.09	8.17	7.77	8.00	7.49	8.09	8.26	11.07	11.08
FeO	9.07	10.68	10.21	10.00	10.32	10.42	12.18	12.03	12.04	11.69	8.98	8.13
MnO	0.31	0.36	0.18	0.35	0.22	0.41	0.20	0.43	0.25	0.40	0.23	0.08
MgO	16.72	14.56	14.92	14.42	14.47	14.70	14.47	14.78	14.67	14.75	14.49	14.96
CaO	11.94	10.57	11.46	10.19	10.56	10.06	10.95	10.43	10.95	10.07	10.69	10.84
Na_2O	1.11	1.31	1.02	1.22	1.09	1.49	0.57	0.53	0.52	0.71	0.75	0.62
K_2O	0.16	0.33	0.11	0.28	0.23	0.35	0.08	0.16	0.08	0.14	0.24	0.01
Cr_2O_3	0.00	0.00	0.03	0.00	0.09	0.00	0.29	0.05	0.01	0.01	0.22	0.57
NiO	0.02	0.04	0.01	0.00	0.00	0.01	0.02	0.00	0.00	0.00	0.00	0.02
Total	97.45	97.49	96.63	96.70	96.56	96.84	97.42	97.14	97.86	96.72	97.85	98.79
Fe_2O_3	3.73	4.34	3.39	4.02	4.36	5.29	8.44	10.04	8.53	10.86	5.38	5.01
FeO	5.71	6.78	7.16	6.38	6.40	5.66	4.58	3.00	4.36	1.92	4.14	3.62
Total	99.95	100.04	99.06	99.21	99.10	99.48	100.39	100.27	100.85	99.94	100.55	101.47
a.p.f.u.												
Si	7.224	7.182	7.154	7.244	7.226	7.201	7.076	7.114	7.125	7.058	6.966	6.910
Ti	0.062	0.116	0.091	0.121	0.069	0.099	0.054	0.072	0.038	0.055	0.116	0.225
Al (iv)	0.776	0.818	0.846	0.756	0.774	0.799	0.924	0.886	0.875	0.942	1.034	1.090
Al (vi)	0.301	0.495	0.476	0.597	0.596	0.502	0.407	0.356	0.460	0.427	0.782	0.703
Fe^{3+}	0.397	0.462	0.365	0.429	0.467	0.565	0.897	1.063	0.899	1.149	0.563	0.518
Fe^{2+}	0.676	0.803	0.857	0.758	0.761	0.673	0.541	0.352	0.511	0.226	0.482	0.416
Mn	0.037	0.044	0.022	0.042	0.027	0.049	0.024	0.051	0.030	0.048	0.027	0.009
Mg	3.525	3.076	3.183	3.052	3.069	3.112	3.044	3.100	3.062	3.093	3.005	3.064
Ca	1.809	1.604	1.757	1.550	1.610	1.531	1.655	1.572	1.643	1.518	1.594	1.595
Na	0.304	0.361	0.284	0.335	0.301	0.409	0.156	0.143	0.141	0.193	0.202	0.165
K	0.030	0.059	0.021	0.051	0.041	0.064	0.014	0.029	0.014	0.025	0.043	0.001
Cr	0.000	0.000	0.004	0.000	0.010	0.000	0.032	0.006	0.001	0.001	0.024	0.062
Ni	0.002	0.005	0.001	0.000	0.000	0.001	0.003	0.000	0.000	0.000	0.000	0.003
Total	15.143	15.024	15.062	14.937	14.952	15.004	14.825	14.745	14.797	14.737	14.839	14.761
Ca (B)	1.27	1.64	1.14	1.50	1.32	1.84	0.65	0.69	0.59	0.85	0.99	0.63
(Na + K) (A)	0.14	0.06	0.06	0.05	0.04	0.06	0.01	0.03	0.01	0.03	0.04	0.00
Sum of S2	13.000	13.000	13.000	13.000	13.000	13.000	13.000	13.000	13.000	13.000	13.000	13.000
Mg#	83.9	79.3	78.8	80.1	80.1	82.2	84.9	89.8	85.7	93.2	86.2	88.0
P (GPa)												
Hammarstrom and Zen (1986)	0.26 ± 0.05						0.27 ± 0.05				0.52	0.51
Hollister et al. (1987)	0.25 ± 0.06						0.27 ± 0.05				0.55	0.54
Johnson and Rutherford (1989)	0.20 ± 0.05						0.21 ± 0.02				0.42	0.41

Abbreviations, Mhb: magnesio-hornblende (abbreviation for mineral name is from Whitney and Evans, 2010). Mineral classification is from Leake et al. (1997). Major element oxides are in wt.%. Atoms per formula units (a.p.f.u) are calculated based on 23 equivalent oxygens with Fe^{2+}/Fe^{3+} (and FeO/Fe_2O_3) estimation assuming 13 cations excluding Ca, Na, and K. Mg# = 100 × Mg/(Mg + Fe^{2+}).

observed for clinopyroxenes from Group 1 basalts, Ti, Na and Al are negatively correlated with increasing Mg#.

It is commonly accepted that clinopyroxene compositions represent a suitable indicator of the magmatic affinity of basalts from different tectonic settings, as well as from different ophiolitic types (e.g., Leterrier et al., 1982; Beccaluva et al., 1989). In fact, the chemical composition of clinopyroxenes, beside to be controlled by crystal-chemical constrain, is also strongly influenced by the composition of magmas from which they crystallize. Using Ti−(Ca + Na), (Ti + Cr)−Ca, and Al−Ti covariation diagrams of Leterrier et al. (1982) clinopyroxenes from Group 1 pillow lavas plot in the fields for tholeiitic-type volcanic arc basalts (Fig. 10). Accordingly, in the TiO_2−SiO_2−Na_2O discrimination diagram of Beccaluva et al. (1989) they plot in the fields for volcanic arc tholeiites (not shown). In contrast, clinopyroxene from Group 2 pillow lavas plot in the field for CA basalts in the diagram of Fig. 10.

7.2. Spinel

Fresh primary chromian spinels were found in samples of Group 1 pillow lavas from both Nain and Ashin ophiolites. In contrast, no spinels were found in Group 2 basalts and in the Nain sheeted dyke series. Representative analyses of chromian spinels are given in Supplementary Table 1. Chromian spinels occurring in pillow lava basalts from the Nain and Ashin ophiolites show quite similar chemical compositions (Supplementary Table 1) and therefore they will be hereafter described as a whole. In the Cr−Al−Fe^{3+} classification diagram (Stevens, 1944), spinels can be classified as Al-chromites (not shown). They are characterized by 1:1 replacement of chromite end-member [$Fe(Cr, Fe^{3+})_2O_4$] by the spinel end-member [$MgAl_2O_4$]. The proportions of these two end-members range from 1.2 spinel - 1.8 chromite to 1.4 spinel - 1.6 chromite. These minerals are characterized by variable, but generally low Al_2O_3 contents (16.44−23.70 wt.%) and moderate Cr_2O_3 contents

Please cite this article as: Pirnia, T et al., Cretaceous tectonic evolution of the Neo-Tethys in Central Iran: Evidence from petrology and age of the Nain-Ashin ophiolitic basalts, Geoscience Frontiers, https://doi.org/10.1016/j.gsf.2019.02.008

(42.08–50.21 wt.%). As a consequence, the Cr# is fairly high (54.63–66.83, Fig. 11). MgO contents are relatively low (10.07–12.94 wt.%), whereas FeO contents are relatively high (19.86–23.85 wt.%). TiO_2 contents, though generally low, are highly variable, as they range from 0.16 to 0.56 wt.%. The lowest TiO_2 contents are observed in spinels from most samples of the Nain pillow lava series ($TiO_2 = 0.16–0.35$ wt.%). In contrast, spinels in the Ashin pillow lava basalts, as well as in sample NA421 (Nain pillow lava series) show comparatively higher TiO_2 contents ($TiO_2 = 0.35–0.56$ wt.%). Individual grains commonly show little compositional variation from core to rim. In most samples, spinels have cores slightly richer in Cr_2O_3 and Al_2O_3 than the rims (Supplementary Table 1). In these samples, Cr_2O_3 and Al_2O_3 contents in core are less than ~4 relative percent higher than in rim. Spinels from many samples show MgO, FeO, and TiO_2 contents that are slightly increasing from cores to rims.

It is commonly recognized that the chemical composition of chromian spinel is a sensitive petrogenetic indicator. Indeed, experimental studies have indicated that Al_2O_3 and TiO_2 contents in chromian spinel are strictly controlled by the contents of these elements in the parental melt (e.g., Maurel and Maurel, 1982; Kamenetsky et al., 2001; Rollinson, 2008). In many cases, the chemical composition of chromian spinels has been used for inferring the parental melt composition (e.g., Kepezhinskas et al., 1993; Zhou et al., 1996; Kamenetsky et al., 2001; Rollinson, 2008; Allahyari et al., 2014; Saccani and Tassinari, 2015). In fact, Maurel and Maurel (1982) have proposed an empirical formula for calculating the Al_2O_3 content of the parental melt starting from the Al_2O_3 content in spinel. Similarly, Rollinson (2008) proposed some empirical formulae that relate the Al_2O_3 and TiO_2 content of chromian spinels and in parental melts. In this study, we use the empirical formulae proposed by Rollinson (2008) in order to verify if chromian spinels have crystallized in equilibrium with the liquid composition of their host rocks. Results are shown in Supplementary Table 1. The calculated Al_2O_3 contents in the liquids are, on average, from 0.5 to 1 wt.% higher than those observed in the whole rocks for all samples from the Nain pillow lavas and from sample AS1009 from the Ashin pillow lavas, whereas in the other basalts from the Ashin ophiolites the calculated Al_2O_3 contents are, on average, from 0.4 to 0.7 wt.% lower than those observed in the whole rocks (Supplementary Table 1). In general, the differences between calculated and observed Al_2O_3 values are little and are included within the uncertainty of the methods. Therefore, we can conclude that both Al_2O_3 and TiO_2 contents calculated from spinel compositions are very similar to those observed in the parental rocks. In fact, the differences between calculated and observed TiO_2 contents range from 0 to 0.04 wt.% for all samples (Supplementary Table 1). In summary, the close similarity between calculated and observed Al_2O_3 and TiO_2 contents suggests that chromian spinels have crystallized in equilibrium with the composition of their host rocks. Therefore, their compositions can be plotted in the discrimination diagram in Fig. 11, where it can be seen that chromian spinels from both Nain and Ashin pillow lavas show quite similar compositions and plot within or close to the field for island arc tholeiitic spinels.

7.3. Amphibole

Fresh primary amphiboles were found in few samples of Group 1 rocks in sheeted dykes and pillow lavas from the Nain and Ashin ophiolites, respectively. Chemical compositions of representative fresh amphiboles are given in Supplementary Table 1. All amphiboles have $Ca > 1.50$, $(Na + K) < 0.5$, Si included between 6.5 and 7.5, and $[Mg/(Mg + Fe^{2+})] > 0.5$ (Table 3) and thus they classify as magnesio-hornblende (Leake et al., 1997). Compositional variation for the analyzed amphiboles shows smooth correlation with increasing differentiation (Table 3). This correlation is exemplified by the variation in Mg#, which are 84.9–93.2 in basalts, and 78.8–83.9 in the basaltic andesite. ($Na_2O + K_2O$) contents are slightly lower in amphiboles in basalts (0.59–0.99 wt.%) than in those in the basaltic andesite (1.14–1.84 wt.%). Likewise, the TiO_2 content in amphiboles from the Nain sheeted dyke series is comparatively lower in basalt (0.36–0.68 wt.%) than in the basaltic andesite (0.59–1.14 wt.%). However, the TiO_2 content in amphiboles from these samples is lower than that of amphiboles from the Ashin pillow lavas series, where it ranges from 1.11 to 2.18 wt.%. Amphiboles from the Nain sheeted dyke series are chemically zoned. In fact, TiO_2, Na_2O, and K_2O contents significantly increase from cores to rims (Table 3).

7.4. Geothermobarometers

Due to the limited occurrence of fresh mineral phases, the geothermobarometers based on clinopyroxene composition and the geobarometers based on amphibole composition are the only methods that can be used for estimating crystallization temperatures and pressures for the studied rocks. In fact, we applied the thermobarometric methods proposed by Putirka et al. (2003) and Putirka (2008) based on clinopyroxene–whole rock equilibrium for estimating crystallization temperatures and pressures of the pillow lavas from both Nain and Ashin ophiolites, as only these rocks included fresh clinopyroxenes. Results are shown in Table 2. Unfortunately, no fresh clinopyroxene is preserved in the sheeted dyke basaltic rocks and therefore the temperature of crystallization of these rocks cannot be estimated. Using the method proposed by Putirka (2008), the estimated magmatic temperatures for both Group 1 and Group 2 basalts from different localities are similar and range from 1195 ± 3 °C to 1224 ± 8 °C. Interestingly, the estimated crystallization pressures vary depending on both rock group and locality. The estimated crystallization pressures for the Nain pillow lavas range from 0.22 ± 0.05 to 0.29 ± 0.06 GPa. Relatively higher pressures were estimated for the Group 1 Ashin pillow lavas, being in the range 0.52–0.54 ± 0.01 GPa. However, the highest pressures were estimated for the Group 2 pillow lavas from the Nain pillow lavas (P = 0.61 ± 0.03 GPa).

The magmatic pressure of formation of the Nain sheeted dykes and one pillow lava basalt from the Ashin ophiolites were also calculated using different methods based on the Al-content in amphibole (Hammarstrom and Zen, 1986; Hollister et al., 1987; Johnson and Rutherford, 1989). Results are shown in Table 3. Though these methods were calibrated for different temperature ranges, they gave similar estimated pressures for the analyzed magnesio-hornblendes (see Table 3). The estimated pressures for the Nain sheeted dykes are in the range of 0.20 ± 0.05 – 0.27 ± 0.05 GPa for both basalt and basaltic andesite. No significant differences between pressures estimated from crystal cores and rims were observed. In contrast, the estimated pressures of crystallization for amphiboles in the Ashin pillow lava basalts are comparatively higher, being in the range of 0.51–0.52 GPa. Sample AS1007/2 from the Ashin pillow lava series is the only sample in which both fresh clinopyroxenes and amphiboles can be found. Therefore, a comparison of the crystallization pressures estimated using these minerals can be made. For this sample, pressures estimated using amphibole composition (0.42–0.55 GPa) are very similar to those estimated using clinopyroxene composition (0.52 GPa). According to these calculations, clinopyroxenes in Group 1 Nain pillow lavas were generated in magma chamber(s) at

Please cite this article as: Pirnia, T et al., Cretaceous tectonic evolution of the Neo-Tethys in Central Iran: Evidence from petrology and age of the Nain-Ashin ophiolitic basalts, Geoscience Frontiers, https://doi.org/10.1016/j.gsf.2019.02.008

depths ranging from ~8 to ~11 km, whereas in similar rocks from the Ashin ophiolites clinopyroxenes and amphiboles crystallized at about 19 km depth. In contrast, clinopyroxenes from in Group 2 pillow lavas from the Nain ophiolites crystallized in magma chamber(s) located at ~23 km depth. Crystallization pressures estimated from amphiboles suggest that the Group 1 Nain sheeted dykes were formed at ~8 km depth.

8. Discussion

8.1. Melt petrogenesis and mantle sources

According to many authors (e.g., Pearce and Norry, 1979; Pearce, 1983), the incompatible element composition of basaltic rocks largely depends on the composition and degree of melting of the associated mantle source, whereas it is little influenced by fractional crystallization (e.g., Pearce, 1983). The trace element composition of different magma-types is therefore primarily related to different source characteristics that are associated, in turn, with distinct tectono-magmatic settings of formation. It follows that the chemical characteristics of the different rock-types forming the volcanic and sheeted dyke series of the Nain and Ashin (hereafter, Nain-Ashin) ophiolites can be used for determining the nature and tectonic significance of the magmatic events that occurred in the oceanic sectors of the Neo-Tethys, which surrounded the CEIM. We will therefore focus our petrogenetic discussion to the identification of the possible mantle sources and related tectonic setting of formation of the different rock-groups forming the sheeted dyke and pillow lava units cropping out in the Nain-Ashin ophiolites. Some trace elements contents (e.g., Nb, Th, and REE) and their degree of depletion or enrichment, as well as trace element ratios (e.g., Nb/Yb, Th/Ta, Th/Nb, Ba/Th) are moderately affected by fractional crystallization of predominantly olivine + clinopyroxene + plagioclase. Therefore, in presence of moderate amounts of fractionation, they are believed to represent the elemental ratios in the source (e.g., Allègre and Minster, 1978; Beker et al., 1997). For this reason, the following discussion will be based on the relatively less fractionated basalts and basaltic andesites of the different magmatic groups. Fig. 9a shows that Group 1 (IAT) and Group 2 (CA) rocks plot in the fields for volcanic arc basalts and show variable extents of Th enrichment relative to Nb, which suggest variable addition of subduction-derived components. These rocks are commonly interpreted as originating from partial melting of sub-arc residual peridotites that experienced Nb and Ti depletion during previous partial melting events followed by Ba, Th, and LREE enrichment carried by subduction-derived fluids or melts (e.g., Pearce, 1982, 1983; Gribble et al., 1996; Parkinson and Pearce, 1998). Pearce and Norry (1979) and Beccaluva et al. (1989) suggested that low Ti contents in clinopyroxenes reflect a depleted nature of the mantle source(s) that generated the clinopyroxene parental magma. The generally low Ti content in clinopyroxenes from both Group 1 and Group 2 pillow lavas (Table 2) also support the hypothesis that they crystallized from primary magmas generated from mantle sources, which underwent Ti removal by previous partial melting events (e.g., Hébert and Laurent, 1990).

A method that is commonly used for estimating the degree of depletion (i.e., degree of melting) of the mantle source(s) is to plot a compatible versus an incompatible element. In fact, compatible element abundance is not significantly modified during the progressive mantle source depletion, whereas the abundance of incompatible elements is closely related to source depletion and degree of melting (Pearce, 1982, 1983). We therefore use the Cr vs. Y diagram (Pearce, 1983; Murton, 1989) shown in Fig. 12 for inferring the composition of mantle sources and the degrees of partial melting generating Group 1 and Group 2 rock-types. In this figure, two possible mantle sources are assumed: (1) a depleted mantle lherzolite, which represents residual mantle after ~12% MORB-type melt extraction (lherzolite EP22 from the Pindos ophiolite in Greece); (2) a comparatively more depleted mantle lherzolite, which represents residual mantle after ~20% MORB-type melt extraction (lherzolite A19 from the Othrys ophiolite in Greece). Both these mantle lherzolites were chosen because they did not undergo detectable enrichment in subduction components (Saccani et al., 2017b). However, the model in Fig. 12 is not appropriate for estimating the possible contribution of subduction-derived components to the mantle source(s). Therefore, in order to qualitatively evaluate the different chemical contributions from subduction-derived components, the Ba/Th ratios are plotted vs. Th/Nb ratios (Fig. 13) and we have applied REE modelling in order to find the mantle peridotite compositions, the partial melting degree, and the nature and extent of enrichment in LREE due to subduction-related fluids and/or melts that best fit the compositions of the less fractionated basaltic rocks for each magmatic type (Fig. 14). However, in supra-subduction zone settings, the fluid flux from a subducted slab may be either localized or pervasive, and fluid-mobile trace elements may be added at every melting increment (see Barth et al., 2003). In addition, the compositions and the amounts of subduction-related trace elements incorporated into the overlying mantle wedge depend on a number of factors, such as the mineralogical compositions of the subducting rocks, temperatures, pressures, and distance from a subduction zone (see, for example, Pearce and Parkinson, 1993; Gribble et al., 1996; Elliott, 2003, Mibe et al., 2011). Given these uncertainties, a rigorous quantification of the melting processes (i.e., composition of mantle sources and degrees of partial melting) generating the different rock-types is not possible as the mantle source compositions cannot be constrained in detail. Nonetheless, the semi-quantitative modelling of REE shown in Fig. 14 can place some solid constraints on the petrogenesis of basaltic rocks in subduction-related settings. Some authors have shown that two distinct components from the slab can be identified in island arc lavas. One component is argued to be a melt of the down-going sediment, while the second is a fluid flux derived from the dehydration of the down-going oceanic crust (e.g., Hochstaedter et al., 2001; Elliott, 2003; Ikeda et al., 2016). The most significant material flux from the slab beneath the fore-arc is water, which is initially represented by seawater released during compaction and porosity reduction in sediments and altered oceanic crust, and then by dehydration of clay minerals (e.g., Kelley et al., 2003; Saffer and Tobin, 2011). For this reason, in the models in Fig. 14, the possible contributions from a melt derived from oceanic pelagic sediments (Taylor and McLennan, 1985) and from seawater (Li, 2000) are taken into account. For the sake of consistency, the depleted peridotites used in the models in Fig. 14 are the same used in the model in Fig. 12.

8.1.1. Group 1 pillow lavas

In the Cr-Y model (Fig. 12), Group 1 pillow lavas from the Nain-Ashin ophiolites are compatible with partial melting degrees of a depleted lherzolite mantle source residual after 12% MORB-type melt extraction (lherzolite EP22), which range from ~8% (for samples with relatively higher Y content) to ~15% (for samples with relatively lower Y contents). The Ba/Th enrichment relative to Th/Nb suggests that the mantle sources of these rocks were predominantly influenced by aqueous fluid addition (Fig. 13). The LREE/MREE depleted nature of most samples suggests however that hydration of the sub-arc mantle wedge was accompanied by a moderate transfer of LREE-enriched subduction zone components (e.g., Barth et al., 2003). Therefore, in Fig. 14a a theoretical mantle source has been calculated by adding 0.5% aqueous fluid to the

Please cite this article as: Pirnia, T et al., Cretaceous tectonic evolution of the Neo-Tethys in Central Iran: Evidence from petrology and age of the Nain-Ashin ophiolitic basalts, Geoscience Frontiers, https://doi.org/10.1016/j.gsf.2019.02.008

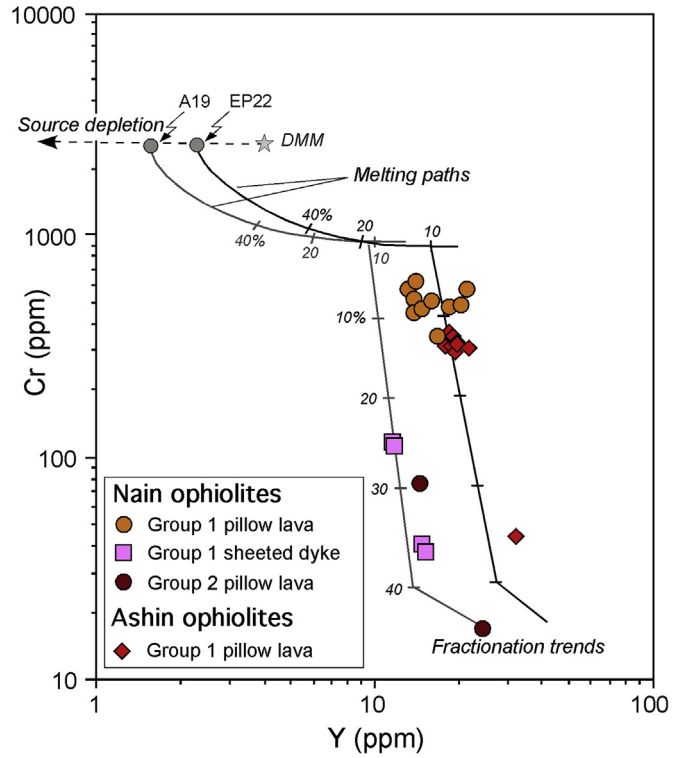

Figure 12. Cr vs. Y diagram of Pearce (1982) and melting models for basaltic pillow lavas and sheeted dykes of the Nain and Ashin ophiolites. Abbreviations, DMM: depleted MORB mantle (Workman and Hart, 2005). Melting paths (with partial melting degrees) for incremental batch melting are calculated according to Murton (1989). The composition of depleted mantle lherzolites assumed as possible mantle sources (A19 and EP22) are from Saccani et al. (2017b). Sources EP22 and A19 represent residual mantle sources after 12% and 20% MORB melt extraction from the DMM source, respectively. The fractional crystallization trends are also shown (tick marks indicate 10% fractional crystallization steps).

depleted lherzolite EP22. According to the results obtained from the model in Fig. 12, the REE composition of Group 1 pillow lavas from the Nain-Ashin ophiolites are compatible with 10%–15% partial melting of the calculated theoretical mantle source. The low

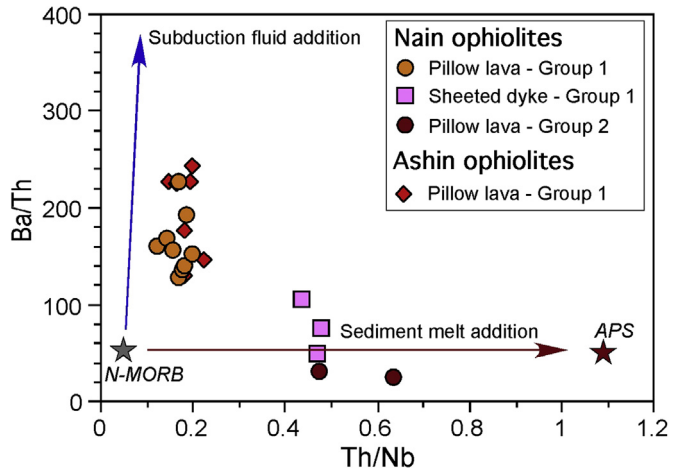

Figure 13. Ba/Th vs. Th/Nb diagram for basaltic pillow lavas and sheeted dykes of the Nain and Ashin ophiolites. Stars indicate the compositions of average pelitic sediments (APS, Taylor and McLennan, 1985) and normal-type mid-ocean ridge basalt (N-MORB, Sun and McDonough, 1989).

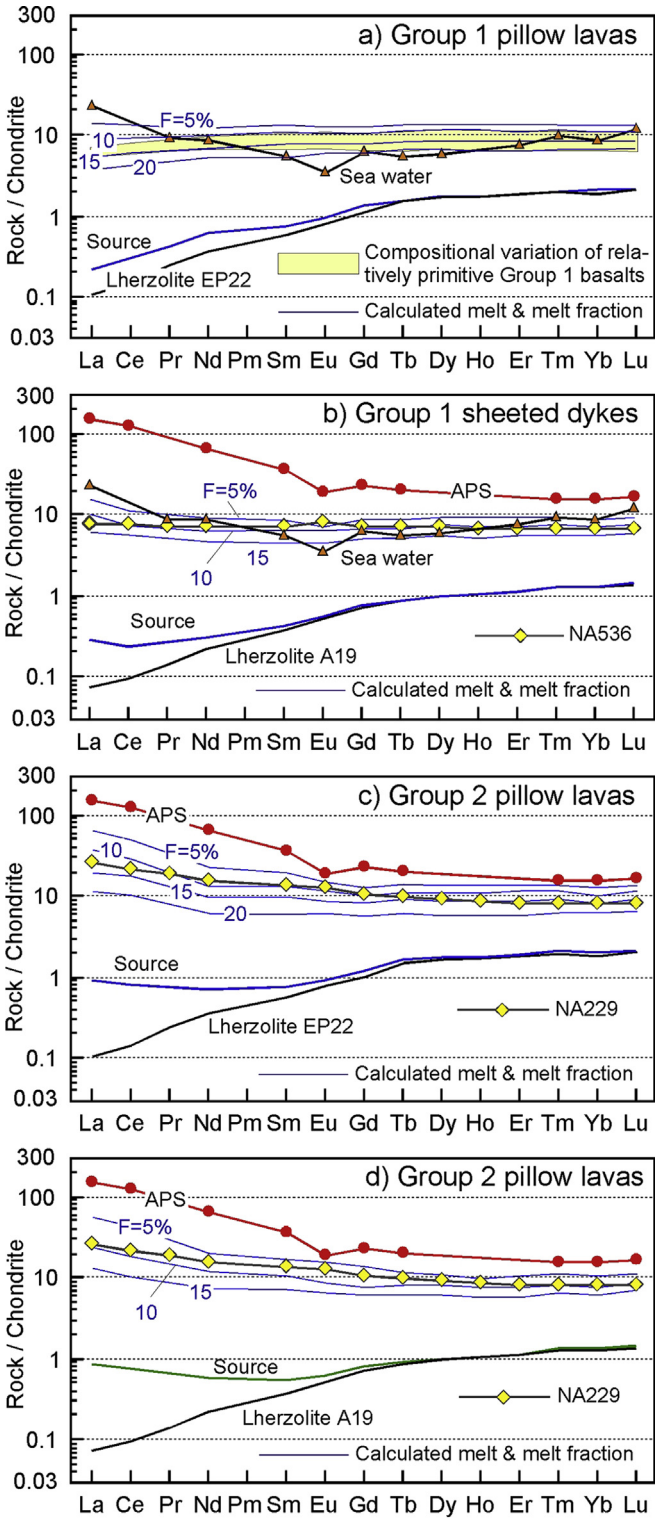

Figure 14. Calculated chondrite-normalized (Sun and McDonough, 1989) rare earth element patterns for parental melts derived from different mantle sources, assuming various degrees of non-modal fractional melting according to the parameters (source modes, melting proportions, etc.) listed in Supplementary Table 2, which also show the compositions of the different inferred mantle sources.

fractionation of HREE with respect to MREE observed in Group 1 (Fig. 7b, d) suggests that the melting of sub-arc mantle source occurred in the spinel-facies.

Please cite this article as: Pirnia, T et al., Cretaceous tectonic evolution of the Neo-Tethys in Central Iran: Evidence from petrology and age of the Nain-Ashin ophiolitic basalts, Geoscience Frontiers, https://doi.org/10.1016/j.gsf.2019.02.008

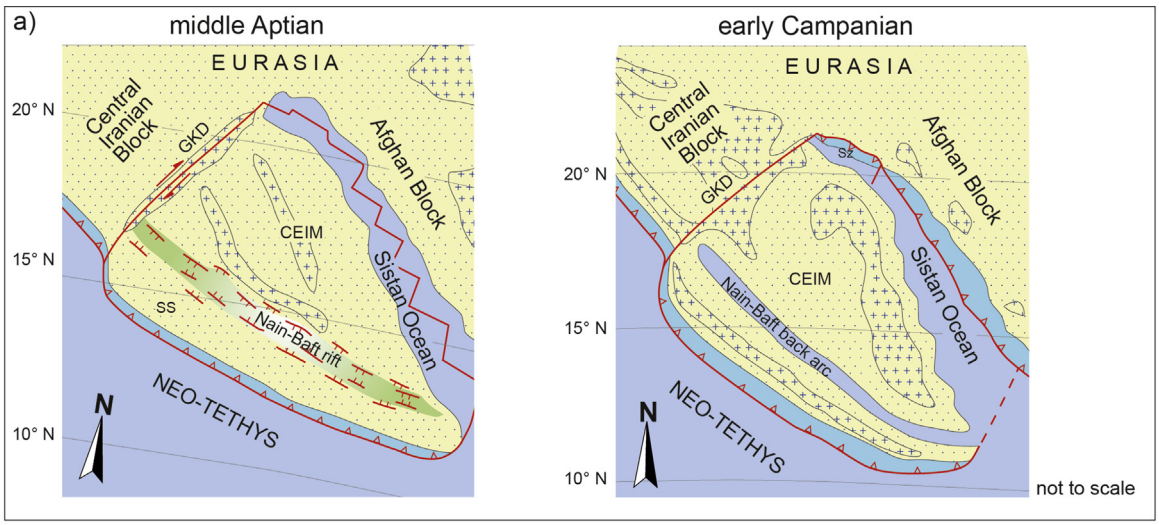

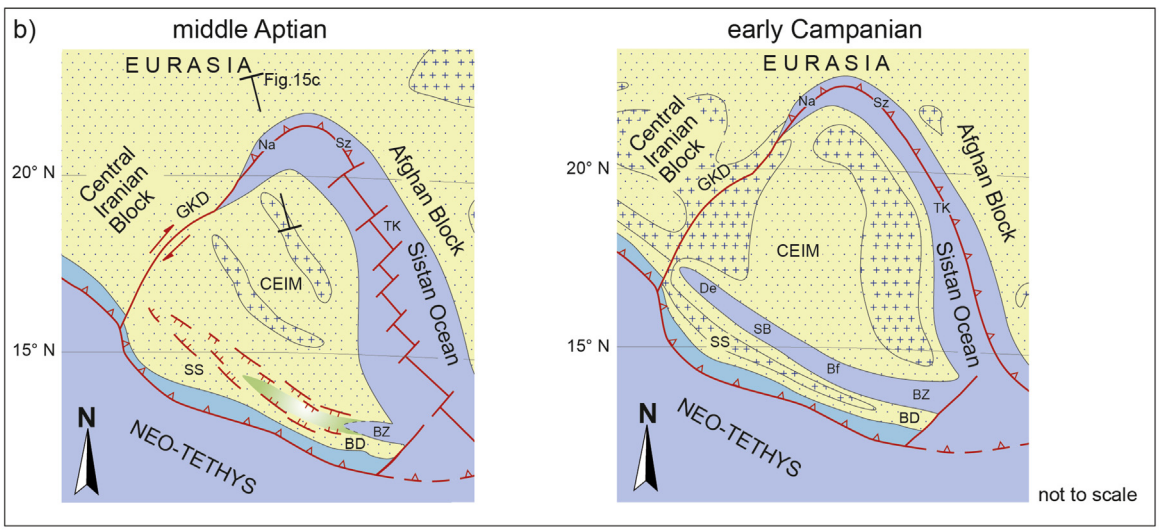

Oceanic domain
- Accretionary wedge
- Oceanic basin

Continental domain
- Rifted basin
- Marine platform and basin
- Exposed land and continental basin

- Active oceanic spreading ridge and transform fault
- Major normal fault
- Active subduction zone
- Major strike-slip fault (arrow indicate the movement component)

Na: Nain
Sz: Sabzevar
SB: Shahr-e-Babak
De: Dehshir
Bf: Baft
BZ: Band-e-Zeyarat
TK: Tchehl Kureh

SS: Sanandaj-Sirjan
BD: Bajgan-Durkan
CEIM: Central-East Iran Microcontinent
GKD: Great Kavir Dorouneh fault system

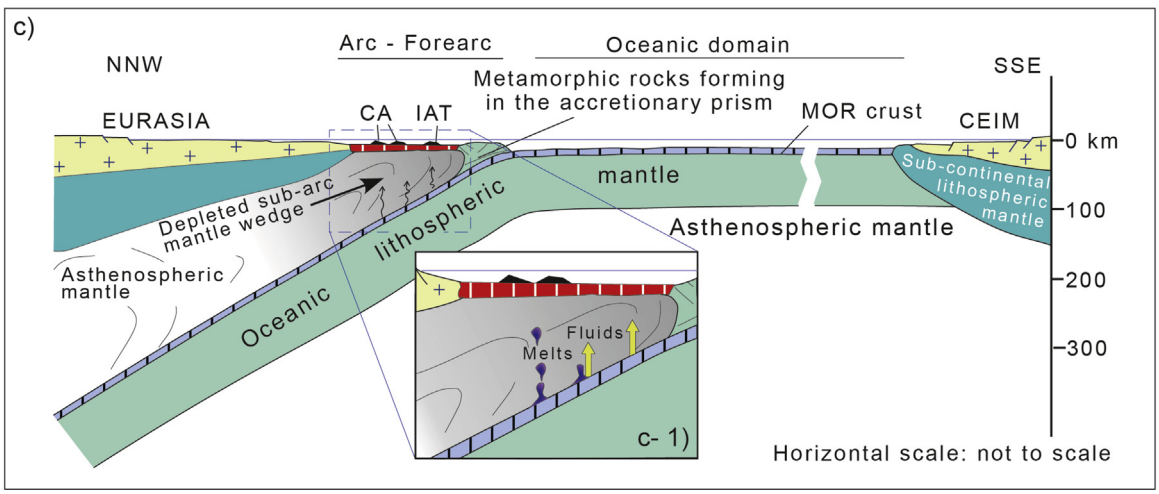

Please cite this article as: Pirnia, T et al., Cretaceous tectonic evolution of the Neo-Tethys in Central Iran: Evidence from petrology and age of the Nain-Ashin ophiolitic basalts, Geoscience Frontiers, https://doi.org/10.1016/j.gsf.2019.02.008

8.1.2. Group 1 sheeted dykes

Although Group 1 sheeted dykes represent slightly fractionated melts, in the Cr-Y model (Fig. 12) these rocks are compatible with ~20% partial melting of the depleted lherzolite EP22, or, alternatively, with ~12% partial melting of the relatively more depleted lherzolite residual after 20% MORB-type melt extraction (lherzolite A19). However, Fig. 13 shows that the mantle source of these rocks was influenced by both aqueous fluid and sediment melt additions. Moreover, these rocks are relatively more enriched in Th with respect to Nb and Ta and show a lower LREE/MREE depletion when compared to similar pillow lava basalts (Figs. 7e and 9a) further suggesting an involvement of a subduction component relatively rich in Th and LREE. For this reason, the REE composition of the possible mantle source for Group 1 sheeted dykes has been calculated by adding 0.1% aqueous fluid components and 0.2% sediment melt component to the depleted lherzolite A19. The model in Fig. 14b shows that the REE composition of the relatively less fractionated Group 1 sheeted dyke basalts is consistent with 10%–12% partial melting of the assumed theoretical mantle source in the spinel stability field.

8.1.3. Group 2 pillow lavas

In the Cr-Y model (Fig. 12), the relatively less fractionated Group 2 basalt (sample NA229) is compatible with ~17% partial melting of the depleted lherzolite EP22, or, alternatively, with ~8% partial melting of the depleted lherzolite A19. The Th/Nb enrichment relative to Ba/Th (Fig. 13), as well as the high La/Yb ratios displayed by these basalts (Table 1, Fig. 7j) suggests that the mantle source of Group 2 rocks was predominantly influenced by a subduction component significantly enriched in Th and LREE. Therefore, we assume that the subduction component that affected the mantle source of Group 2 basalts was likely represented by sediment melt addition (Fig. 13). For the REE models, we therefore calculated two possible theoretical mantle source compositions by adding 0.5% sediment melt to both lherzolite EP22 (Fig. 14c) and lherzolite A19 (Fig. 14d). According to the Cr-Y model (Fig. 12), the REE models show that the REE composition of Group 2 basalt NA229 can be either compatible with 15%–18% partial melting of the depleted lherzolite EP22 (Fig. 14c), or with ~8% partial melting of the relatively more depleted lherzolite A19 (Fig. 14d). With the available data, it not possible to assess in detail which of these models is the most appropriate one for explaining the formation of Group 2 primary melts. In any case, a first order conclusion is that Group 2 primary melts were originated from partial melting of a depleted peridotite residual after 12%–20% MORB-melt extraction, which underwent subsequent incompatible element input due to sediment melt addition. Finally, the low MREE/HREE fractionation of both sample NA229 ($Sm_N/Yb_N = 1.66$) and calculated melts ($Sm_N/Yb_N = 1.33–1.43$) suggest that partial melting occurred in the spinel-facies mantle. In fact, the Sm/Yb ratios calculated for partial melting in the garnet-facies mantle starting from the same mantle compositions would be much higher ($Sm_N/Yb_N > 4.0$) than that observed in Group 2 basalts.

8.2. Tectono-magmatic significance and geodynamic implications

It is widely accepted that the study of igneous rocks incorporated within ophiolitic mélanges may provide robust constraints for the magmatic and geodynamic evolution of the oceanic basins from which they were derived: from continental rifting and break-up to the development of an oceanic lithosphere, its consumption in a converging setting and, finally, ophiolite emplacement (e.g., Floyd et al., 1991; Tankut et al., 1998; Bortolotti et al., 2004). In fact, the petrological evidence presented in Section 8.1 allows us to conclude that pillow lavas and sheeted dykes from the Nain-Ashin ophiolitic mélanges were formed from primary melts generated, in turn, from depleted mantle sources that experienced variable extents of subduction-related metasomatisms prior to melting. Therefore, all these rocks were generated in a volcanic arc tectonic setting. Nonetheless, the different nature of the inferred mantle sources associated with each single rock-group suggests that they were likely formed in different portions of the same volcanic arc setting. The CA nature and the marked influence from sediment melts shown by Group 2 rocks (Figs. 9a and 13) suggest formation in a continental margin volcanic arc or in an intra-oceanic arc characterized by a thick polygenetic crust (see Dilek and Furnes, 2011; Saccani, 2015). In contrast, the island arc tholeiitic affinity of Group 1 rocks and their moderate subduction-type geochemical signature suggest that these rocks were influenced by subduction-released fluids and likely formed in the forearc sector of a volcanic arc setting.

Several models for the geodynamic evolution of the oceanic branches of the Neo-Tethys that were existing in Mesozoic times around the CEIM have been suggested by many authors (e.g., Shojaat et al., 2003; Barrier and Vrielynck, 2008; Shafaii Moghadam et al., 2009; Rossetti et al., 2010; Omrani et al., 2013; Mattei et al., 2014; Shirdashtzadeh et al., 2015). Rahmani et al. (2007) suggested that the Nain ophiolites were formed in an intra-oceanic island arc setting during the Late Cretaceous. Likewise, Ghazi and Hassanipak (2000) and Khalatbari Jafari et al. (2015) suggested a similar tectonic setting of formation for the neighboring Shahr-e-Babak and Dehshir ophiolites, respectively. Unfortunately, these authors did not suggest any hypothesis about the original location of the supposed intra-oceanic arc with respect to the CEIM. Based on geochemical studies on a quite limited number of mafic volcanic rocks from the Nain, Dehshir, Shahr-e-Babak, and Baft ophiolites (Shafaii Moghadam et al., 2009), as well as on the Nain mantle peridotites (Mehdipour Ghazi et al., 2010; Pirnia et al., 2010), these authors have suggested that the Nain-Baft belt ophiolites were formed in a backarc basin. This backarc basin opened in the southern margin of the CEIM in the upper Early Cretaceous and developed in the Late Cretaceous in response to the subduction of the southern branch of the Neo-Tethys below the CEIM (Fig. 15a). The opening of this backarc also resulted in the formation and drifting of the Sanandaj-Sirjan continental block from the CEIM (e.g., Takin, 1972; McCall, 2002; Shahabpour, 2005; Barrier and Vrielynck, 2008).

However, recent paleomagnetic studies in Central Iran were used to reconstruct the history of rotations and latitudinal drift of the CEIM during the Mesozoic and Cenozoic times (Mattei et al., 2012, 2014). These studies indicate that the CEIM underwent two distinct phases of significant counter-clockwise rotation: (1) during the Early Cretaceous and (2) after the Middle-Late Miocene. In particular, the Cenozoic counter-clockwise rotation resulted in a rotation of 20°–35° of the CEIM along of the Great Kavir–Dorouneh fault system. The amount of crustal shortening that could be accommodated by this rotation along right-lateral strike-slip faults is estimated to be ~400 km in length and ~100 km apart. According to Mattei et al. (2012), the effects of this rotation are particularly evident in the Anarak-Nain-Ashin area (Fig. 1a). In

Figure 15. Early and Late Cretaceous paleotectonic schemes of the Central-East Iran microcontinent (CEIM) and surrounding areas. (a) Based on the extant literature data (redrawn from Barrier and Vrielynck, 2008); (b) based on the new data presented in this paper (modified from Barrier and Vrielynck, 2008; Allahyari et al., 2014; Mattei et al., 2014; Saccani et al., 2014); (c) two-dimensional tectonic reconstruction of the subduction in the transect from the northern CEIM to the southern Eurasian continental margin at Early Cretaceous times. Abbreviations, MOR: mid-ocean ridge; HP-LT: high pressure-low temperature; IAT: island arc tholeiite; CA: calc-alkaline.

Please cite this article as: Pirnia, T et al., Cretaceous tectonic evolution of the Neo-Tethys in Central Iran: Evidence from petrology and age of the Nain-Ashin ophiolitic basalts, Geoscience Frontiers, https://doi.org/10.1016/j.gsf.2019.02.008

particular, these authors have shown that the Paleozoic continental basement in the Anarak area and the overlying Mesozoic ophiolites of Nain and Ashin were displaced along the Great Kavir–Dorouneh fault system, from a northeasternmost original location as a result of the Cenozoic phase of the counter-clockwise rotation of the CEIM.

The overall geochemical characteristics of the Nain-Ashin volcanic rocks and dykes show close similarities with their equivalents from the Sabzevar ophiolites, which were interpreted as formed in a volcanic arc setting (Lensch et al., 1979; Baroz and Macaudiere, 1984; Shojaat et al., 2003; Rezaei et al., 2018) (Fig. 5). In contrast, they show significantly different compositions compared to the volcanic rocks from the Baft, Dehshir, and Shar-e-Babak ophiolites, which have been interpreted as formed in a backarc basin (Shafaii Moghadam et al., 2009) (Fig. 5). A recent petrological study on the mantle lherzolites from the Nain ophiolites has shown that they do not represent relicts of backarc mantle peridotites. Rather, they represent sub-continental mantle (i.e., the Continental Margin ophiolites of Dilek and Furnes, 2011; Saccani et al., 2015) exhumed at an Iberia-type ocean-continent transition zone (Pirnia et al., 2018). Finally, the radiolarian biostratigraphic data presented in this paper indicate that the Ashin volcanic arc rocks were formed during the Aptian.

All these data show robust evidence in contrast with the hypothesis of formation of the Nain-Ashin ophiolites in the Nain-Baft backarc basin in the southwest of the CEIM during the Late Cretaceous (Barrier and Vrielynck, 2008; Shafaii Moghadam et al., 2009). For example, the Continental Margin peridotites (Pirnia et al., 2018) are genetically unrelated to the chromitite-bearing harzburgites, as well as to the volcanic rocks and dykes cropping out in the Nain-Ashin ophiolites. In fact, the association of chromite-bearing harzburgites and volcanic arc rocks cropping out in the Nain-Ashin ophiolites point out for their formation in a supra-subduction tectonic setting during the closure phase of the oceanic basin. In contrast, Continental Margin lherzolites, such as the Nain lherzolites (Pirnia et al., 2018) typically represent subcontinental mantle exhumed during the continental rifting that precede the early stage of formation of a subduction-unrelated oceanic basin (see Dilek and Furnes, 2011; Saccani et al., 2015).

A possible tectono-magmatic model that can explain the formation in the Early Cretaceous of the different volcanic arc rock-types in the Nain-Ashin ophiolites is shown in Fig. 15b and c. In this model, we suggest that, similar to the Sabzevar ophiolites, the Nain-Ashin volcanic arc rocks were formed in a volcanic arc that was active between the northern margin of the CEIM and the southern margin of Eurasia during the Early Cretaceous (Fig. 15b). Based on evidence shown by Mattei et al. (2012, 2014), we postulate that this volcanic arc was associated with the subduction below the Eurasian margin of the Sabzevar-Nain-Ashin sector of the Sistan Ocean (Fig. 15c), which was driven, in turn, by the Early Cretaceous counter-clock wise rotation and drifting toward the northwest of the CEIM. In the same times, the Sistan Ocean was still opening to the west of the CEIM, as suggested by radiolarian biostratigraphic data (Babazadeh and De Wever, 2004), whereas the southern margin of the CEIM (i.e., the future Sanandaj-Sirjan zone) was characterized by a volcanic arc activity associated with the subduction of the southern branch of the Neo-Tethys below the CEIM (Fig. 15b). To the north of this arc, a continental rifting started in the Early Cretaceous in response to this subduction and evolved to a narrow backarc basin only in the Late Cretaceous (Fig. 15b). The opening of this backarc basin resulted in the formation of the backarc-type oceanic lithosphere now represented by the Dehshir, Shahr-e-Babak, and Baft ophiolites (e.g., Barrier and Vrielynck, 2008; Shafaii Moghadam et al., 2009).

The geochemical models discussed in Section 8.1 show that the Nain-Ashin volcanic rocks and dykes originated from partial melting of depleted peridotites (Fig. 12) that experienced variable extent of chemical contributions from the subducting slab (Figs. 13 and 14). The inferred magmatic evolution in the subduction system between the CEIM and the Eurasian plate is shown in Fig. 15c. The material released from the subducting slab is represented by water beneath the fore-arc and by melts from the down-going subducting sediments beneath the arc (e.g., Hochstaedter et al., 2001; Elliott, 2003; Ikeda et al., 2016). The contribution from the subducting slab vary from pure aqueous fluid flux for IAT pillow lavas to a mix of aqueous fluids and sediment melts for IAT sheeted dykes, and only sediment melts for CA pillow lavas (Fig. 15c). We therefore postulate that the different magmatic products found in the Nain-Ashin ophiolites were erupted in different sectors of an arc-forearc setting (Fig. 15c). As commonly observed in convergent plate settings, aqueous fluids are basically released from the slab beneath the fore-arc region, whereas sediment melts are most likely generated beneath the arc (e.g., Hochstaedter et al., 2001; Elliott, 2003; Kelley et al., 2003; Saffer and Tobin, 2011; Ikeda et al., 2016). As a consequence we can postulate that IAT rocks were generated in the forearc and outer arc sectors, whereas, CA rocks were generated in the arc sector. The pressure of crystallization estimated for the different volcanic rock-types also support this conclusion. In fact, the estimated crystallization depths increase from IAT pillow lavas (8–19 km) to CA pillow lavas (~23 km). The Mesozoic ophiolites of Nain-Ashin were emplaced before the Paleocene, since they are covered by Paleocene–Eocene sedimentary rocks (Shirdashtzadeh et al., 2011, and references therein).

9. Conclusions

The Nain and Ashin ophiolites consist of “Coloured Mélange” units. They are emplaced onto the westernmost corner of the Central-East Iran microcontinent (CEIM) at the intersection of two regional-scale transcurrent fault systems, which have been discontinuously active from the Jurassic to present-day. Though volumetrically subordinate these mélanges incorporate distinct tectonic slices consisting of sheeted dykes and pillow lavas. Locally, pillow lavas are stratigraphically associated with radiolarian cherts. The main conclusions obtained from the petrological study of volcanic rocks and dykes, as well as biochronological investigation of the associated cherts can be summarized as follows.

(1) Volcanic rocks and dykes are largely represented by basalts. Based on whole rock geochemistry and mineral chemistry, these rocks can be divided into two geochemical groups: (i) The sheeted dykes and most of the pillow lavas show island arc tholeiitic (IAT) affinity with relatively low contents of Th, Nb, Ta, Ti, coupled with LREE/MREE depletion ($(La/Sm)_N = 0.5–1.0$); (ii) A few pillow lavas from the Nain ophiolites show calc-alkaline (CA) affinity, with comparatively high Th, U, and LREE/MREE ratios ($(La/Sm)_N = 1.9–2.6$) coupled with low Nb and Ta contents.

(2) Cr-Y modeling indicates that both IAT and CA rocks derived from moderate degrees (~8%–~15%) of partial melting of depleted mantle sources, which experienced previous MORB-melt extraction. REE modeling indicates that mantle sources underwent variable extent of enrichment in subduction-derived components consisting of pure aqueous fluids (for most IAT basalts), pure sediment melts (for CA rocks) and a mix of aqueous fluids and sediment melts (for some IAT sheeted dykes). These conclusions suggest that the studied rocks were formed in an arc-forearc tectonic setting. The radiolarian

Please cite this article as: Pirnia, T et al., Cretaceous tectonic evolution of the Neo-Tethys in Central Iran: Evidence from petrology and age of the Nain-Ashin ophiolitic basalts, Geoscience Frontiers, https://doi.org/10.1016/j.gsf.2019.02.008

assemblage in the cherts associated with pillow basalts from the Ashin ophiolites suggest that this volcanic arc setting was active in the Early Cretaceous.

(3) We propose a new model for the Cretaceous tectonic evolution of the CEIM and surrounding Neo-Tethyan oceanic basins. This model implies that the Nain-Ashin volcanic rocks and dykes were formed, similar to the Sabzevar ophiolites, in a volcanic arc setting located between the northern margin of the CEIM and the southern margin of Eurasia and forming the northwestern prolongation of the Sistan Ocean. This conclusion is also based on recent studies, which have shown that the CEIM underwent a considerable counter-clockwise rotation in the Cenozoic. Therefore, it is reasonable to assume that the Nain-Ashin ophiolites, together with the underlying continental basement, have been displaced in their present day position, along the Great Kavir-Dorouneh fault system, from their northeasternmost original location. Our new model is significantly differing from the currently most accepted hypothesis, which implies that the Nain ophiolites formed, together with the Baft ophiolites, in a backarc basin (the so-called Nain-Baft backarc basin) located to the south of the CEIM during the Late Cretaceous.

Acknowledgments

This work was supported by the Horizon 2020 MARIE SKŁODOWSKA-CURIE project CIAO (Project No. 658591) granted to T. Pirnia, as well as by the FIR-2016 Project from the Ferrara University (Project leader E. Saccani). We would like to thank Dr. F. Zaccarini (University of Leoben, Austria) for her assistance during the electron microprobe analysis. R. Tassinari (University of Ferrara) is acknowledged for his technical support with whole rock chemical analyses. This paper greatly benefited from the insightful and constructive comments by K. Allahyari and an anonymous reviewer. We are also very grateful to Dr. V. Samuel and Prof. M. Santosh for their editorial help.

Supplementary data

Supplementary data to this article can be found online at https://doi.org/10.1016/j.gsf.2019.02.008.

References

Allahyari, K., Saccani, E., Rahimzadeh, B., Zeda, O., 2014. Mineral chemistry and petrology of highly magnesian ultramafic cumulates from the Sarve-Abad (Sawlava) ophiolites (Kurdistan, NW Iran): new evidence for boninitic magmatism in intra-oceanic fore-arc setting in the Neo-Tethys between Arabia and Iran. Journal of Asian Earth Sciences 79, 312–328.

Allègre, C.J., Minster, J.F., 1978. Quantitative models of trace element behaviour in magmatic processes. Earth and Planetary Science Letters 38, 1–25.

Angiboust, S., Agard, P., de Hoog, J.C.M., Omrani, J., Plunder, A., 2013. Insights on deep, accretionary subduction processes from the Sistan ophiolitic "mélange" (Eastern Iran). Lithos 156–159, 139–158.

Babazadeh, S.A., De Wever, P., 2004. Radiolarian Cretaceous age of soulabest radiolarites in ophiolite suite of eastern Iran. Bulletin de la Societé géologique de France 175, 121–129.

Baroz, F., Macaudiere, J., 1984. La serie volcanosedimentaire du chainon ophiolitique de Sabzevar (Iran). Ofioliti 9, 3–26.

Barrier, E., Vrielynck, B., 2008. Palaeotectonic Maps of the Middle East, Tectono-Sedimentary Palinspastic Maps from Late Norian to Piacenzian. Commission for the Geological Map of the World (CGMW), Paris.

Barth, M.G., Mason, P.R.D., Davies, G.R., Dijkstra, A.H., Drury, M.R., 2003. Geochemistry of the othris ophiolite, Greece: evidence for refertilization? Journal of Petrology 44, 1759–1785.

Baumgartner, P.O., Bjørklund, K.R., Caulet, J.P., De Wever, P., Kellogg, D., Labracherie, M., Nakaseko, K., Nishimura, A., Schaaf, A., Schimdt-Effing, R., Yao, A., 1981. Eurorad II, 1980. Second European meeting of radiolarian paleontologists: current research on Cenozoic and Mesozoic radiolarians. Eclogae Geologicae Helvetiae 74, 1027–1061.

Beccaluva, L., Macciotta, G., Piccardo, G.B., Zeda, O., 1989. Clinopyroxene compositions of ophiolite basalts as petrogenetic indicator. Chemical Geology 77, 165–182.

Beker, J.A., Menzies, M.A., Thirlwall, M.F., Macpherson, C.G., 1997. Petrogenesis of Quaternary intraplate volcanism, Sana'a, Yemen: implications for plume-lithosphere interaction and polybaric melt hybridization. Journal of Petrology 38, 1359–1390.

Berra, F., Zanchi, A., Angiolini, L., Vachard, D., Vezzoli, G., Zanchetta, S., Bergomi, M., Javadi, H.R., Kouhpeyma, M., 2017. The upper Palaeozoic Godar-e-Siah Complex of Jandaq: evidence and significance of a North Palaeotethyan succession in Central Iran. Journal of Asian Earth Sciences 138, 272–290.

Bortolotti, V., Chiari, M., Kodra, A., Marcucci, M., Mustafa, F., Principi, G., Saccani, E., 2004. New evidence for Triassic MORB magmatism in the northern Mirdita Zone ophiolites (Albania). Ofioliti 29, 243–246.

Camp, V.E., Griffis, R.J., 1982. Character, genesis and tectonic setting of igneous rocks in the Sistan suture zone, eastern Iran. Lithos 15, 221–239.

Danelian, T., 2008. Diversity and biotic changes of Arcaeodictyomitrid Radiolaria from the Aptian/Albian transition (OAE1b) of southern Albania. Micropaleontology 54, 3–13.

Davoudzadeh, M., 1972. Geology and Petrology of the Area North of Nain, Central Iran. Geological Survey of Iran, p. 89. Report No. 1.

Delavari, M., Dolati, A., Marroni, M., Pandolfi, L., Saccani, E., 2016. Association of MORB and SSZ ophiolites along the shear zone between coloured mélange and bajgan complexes (North Makran, Iran): evidence from the sorkhband area. Ofioliti 41, 21–34. https://doi.org/10.4454/ofioliti.v41i1.440.

Desmons, J., Beccaluva, L., 1983. Mid-ocean ridge and island-arc affinities in ophiolites from Iran: Palaeographic implications. Chemical Geology 39, 39–63.

De Wever, P., 1982. Radiolaires du Trias et du Lias de la Téthys (systématique, stratigraphie). Société Géologique du Nord 7, 1–600.

Dilek, Y., Furnes, H., 2011. Ophiolite genesis and global tectonics: geochemical and tectonic fingerprinting of ancient oceanic lithosphere. Geological Society of America Bulletin 123, 387–411.

Droop, G.T.R., 1987. A general equation for estimating Fe^{3+} concentrations in ferromagnesian silicates and oxides from microprobe analyses, using stoichiometric criteria. Mineralogical Magazine 51, 431–435.

Dumitrica, P., 1970. Cryptocephalic and cryptothoracic Nassellaria in some Mesozoic deposits of Romania. Revue Roumaine de Géologie Géophysique et Géographie (série Géologie) 14, 45–124.

Elliott, T., 2003. Tracers of the slab. In: Eiler, J. (Ed.), Inside the Subduction Factory, vol. 138. Geophysical Monograph Series AGU, Washington DC, pp. 23–45.

Ewart, A., Bryan, W.B., Chappell, B.W., Rudnick, R.L., 1994. Regional geochemistry of the Lau-Tonga arc and backarc systems. In: Hawkins, J., Parson, L., Allan, J., et al. (Eds.), Proceedings of the Ocean Drilling Program. Scientific Results 135. Ocean Drilling Program, College Station, TX, pp. 385–425.

Floyd, P.A., Kelling, G., Gökçen, S.L., Gökçen, N., 1991. Geochemistry and tectonic environment of basaltic rocks from the Misis Ophiolitic Melange, south Turkey. Chemical Geology 89, 263–280.

Ghazi, A.M., Hassanipak, A.A., 2000. Petrology and geochemistry of the shahr-babak ophiolite, central Iran. In: Dilek, Y., Moores, E., Elthon, D., Nicolas, A. (Eds.), Ophiolites and Oceanic Crust; New Insights from Field Studies and the Ocean Drilling Program, vol. 349. Geological Society of America, Special Papers, pp. 485–497.

Gribble, R.F., Stern, R.J., Bloomer, S.H., Stüben, D., O'Hearn, T., Newman, S., 1996. MORB mantle and subduction components interact to generate basalts in the southern Mariana Trough back-arc basin. Geochimica et Cosmochimica Acta 60, 2153–2166.

Hammarstrom, J.M., Zen, E-an, 1986. Aluminium in hornblende: an empirical igneous geobarometer. American Mineralogist 71, 1297–1313.

Hassanipak, A.A., Ghazi, A.M., 2000. Petrochemistry, $^{40}Ar-^{39}Ar$ Ages and Tectonics of the Naien Ophiolite, Central Iran. GSA Annual Meeting, Reno, Nevada, pp. 237–238.

Hastie, A.R., Kerr, A.C., Pearce, J.A., Mitchell, S.F., 2007. Classification of altered volcanic island arc rocks using immobile trace elements: development of the Th–Co discrimination diagram. Journal of Petrology 48, 2341–2357.

Hébert, R., Laurent, R., 1990. Mineral chemistry of the plutonic section of the Troodos ophiolite: new constraints for genesis of arc-related ophiolites. In: Malpas, J., Moores, E., Panayiotou, A., Xenophontos, C. (Eds.), Ophiolites-Oceanic Crustal Analogues. Proceedings of Troodos Ophiolite Symposium. Geological Survey of Cyprus, pp. 149–163.

Hébert, R., Huot, F., Wang, C., Liu, Z., 2003. Yarlung Zangbo ophiolites (Southern Tibet) revisited: geodynamic implications from the mineral record. Geological Society London Special Publications 218, 165–190.

Hochstaedter, A., Gill, J., Peters, R., Broughton, P., Holden, P., Taylor, B., 2001. Across-arc geochemical trends in the Izu-Bonin arc: contributions from the subducting slab. Geochemistry, Geophysics, Geosystems 2. Paper number 2000GC000105. https://doi.org/10.1029/2000GC000105.

Hollister, L.S., Grissom, G.C., Peters, E.K., Slowell, H.H., Sisson, V.B., 1987. Confirmation of the empirical correlation of Al in hornblende with pressure of solidification of calc-alkaline plutons. American Mineralogist 72, 231–239.

Ikeda, Y., Nagao, K., Ishii, T., Matsumoto, D., Stern, R.J., Kagami, H., Arima, M., Bloomer, S.H., 2016. Contributions of slab fluid and sediment melt components to magmatism in the Mariana Arc-Trough system: evidence from geochemical compositions and Sr, Nd, and noble gas isotope systematics. Island Arc 25, 253–273.

Johnson, M.C., Rutherford, M.J., 1989. Experimental calibration of the aluminum-in-hornblende geobarometer with application to Long Valley Caldera (California) volcanic rocks. Geology 17, 837–841.

Kamenetsky, V.S., Crawford, A.J., Meffre, S., 2001. Factors controlling chemistry of magmatic spinel: an empirical study of associated olivine, Cr-spinel and melt inclusions from primitive rocks. Journal of Petrology 42, 655–671.

Kelley, K.A., Plank, T., Ludden, J., Staudigel, H., 2003. Composition of altered oceanic crust at ODP Sites 801 and 1149. Geochemistry, Geophysics, Geosystems 4, 1–21.

Kepezhinskas, P.K., Taylor, R.N., Tanaka, H., 1993. Geochemistry of plutonic spinels from the north Kamchatka arc: comparisons with spinels from other tectonic settings. Mineralogical Magazine 57, 575–589.

Khalatbari Jafari, M., Sepehr, H., Mobasher, K., 2015. Tectonomagmatic evolution of the south Dehshir ophiolite, Central Iran. Geological Magazine 153, 557–577. https://doi.org/10.1017/S0016756815000618.

Lachance, G.R., Traill, R.J., 1966. A practical solution to the matrix problem in X-ray analysis. Canadian Journal of Spectroscopy 11, 43–48.

Leake, B.E., Woolley, A.R., Arps, C.E.S., Birch, W.D., Gilbert, M.C., Grice, J.D., Hawthorne, F.C., Kato, A., Kisch, H.J., Krivovichev, V.G., Linthout, K., Laird, J., Mandarino, J.A., Maresch, W.V., Nickel, E.H., Rock, N.M.S., Schumacher, J.C., Smith, D.C., Stephenson, N.C.N., Ungaretti, L., Whittaker, E.J.W., Youzhi, G., 1997. Nomenclature of amphiboles: report of the subcommittee on amphiboles of the International Mineralogical Association, commission on new minerals and mineral names. Canadian Mineralogist 35, 219–246.

Lensch, G., Davoudzadeh, M., 1982. Ophiolites in Iran. Neues Jahrbuch für Geologie und Paläontologie Monatsheft 5, 306–320.

Lensch, G., Mihm, A., Alavi-Tehrani, N., 1979. Major element geochemistry of the ophiolites north of Sabzevar (Iran). Neues Jahrbuch für Geologie und Paläontologie Monatsheft 7, 415–447.

Leterrier, J., Maury, R.C., Thonon, P., Girard, D., Marchal, M., 1982. Clinopyroxene composition as a method of identification of the magmatic affinities of paleo-volcanic series. Earth and Planetary Science Letters 59, 139–154.

Li, G., 2000. Petrologic features and genesis of Cenozoic volcanic rocks, Qiang-tang area, northern Tibetan Plateau. Geology Geochemistry 28, 38–44.

Mattei, M., Cifelli, F., Muttoni, G., Zanchi, A., Berra, F., Mossavvari, F., Eshraghi, S.A., 2012. Neogene block-rotation in Central Iran: evidence from paleomagnetic data. Geological Society of America Bulletin 124, 943–956. https://doi.org/10.1130/B30479.1.

Mattei, M., Cifelli, F., Muttoni, G., Rashid, H., 2014. Post-cimmerian (Jurassic–Cenozoic) paleogeography and vertical axis tectonic rotations of Central Iran and the Alborz Mountains. Journal of Asian Earth Sciences 102, 92–101. https://doi.org/10.1016/j.jseaes.2014.09.038.

Maurel, C., Maurel, P., 1982. Étude expérimental de la distribution de l'aluminium entre bain silicate basique et spinelle chromifère. Implications pétrogénétiques: teneur en chrome des spinelles. Bulletin de Mineralogie 105, 197–202.

McCall, G.J.H., 2002. A summary of the geology of the Iranian Makran. In: Clift, P.D., Kroon, D., Gaedicke, C., Craig, J. (Eds.), The Tectonic and Climatic Evolution of the Arabian Sea Region. Geological Society of London, Special Publication 195, pp. 147–204.

Mehdipour Ghazi, J., Moazzen, M., Rahgoshay, M., Shafaii Moghadam, H., 2010. Mineral chemical composition and geodynamic significance of peridotites from Nain ophiolite, central Iran. Journal of Geodynamic 49, 261–270.

Mibe, K., Kawamoto, T., Matsukage, K.N., Fei, Y., Ono, S., 2011. Slab melting versus slab dehydration in subduction-zone magmatism. Proceedings of the National Academy of Sciences 108, 8177–8182.

Morimoto, N., 1989. Nomenclature of pyroxenes. Canadian Mineralogist 27, 143–156.

Murton, B.J., 1989. Tectonic controls on boninite genesis. In: Saunders, A.D., Norry, M.J. (Eds.), Magmatism in the Ocean Basins, vol. 42. Geological Society of London, Special Publications, pp. 347–377.

O'Dogherty, L., 1994. Biochronology and Paleontology of mid-Cretaceous radiolarians from northern Apennines (Italy) and betic cordillera (Spain). Mémoires de Géologie (Lausanne) 21, 1–415.

OO'Dogherty, L., Carter, E.S., Dumitrica, P., Goričan, Š., De Wever, P., Bandini, A.N., Baumgartner, P.O.S., Matsuoka, A., 2009. Catalogue of Mesozoic radiolarian genera. Part 2: Jurassic–Cretaceous. Geodiversitas 31, 271–356.

O'Dogherty, L., Gorican, S., Gawlick, H.J., 2017. Middle and late Jurassic radiolarians from the neotethys suture in the eastern alps. Journal of Paleontology 91, 25–72.

Omrani, H., Moazzen, M., Oberhänsli, R., Altenberger, U., Lange, M., 2013. The Sabzevar blueschists of the North-Central Iranian micro-continent as remnants of the Neotethys related oceanic crust subduction. International Journal of Earth Sciences 102, 1491–1512.

Parkinson, I.J., Pearce, J.A., 1998. Peridotites from the Izu-Bonin-Mariana forarc (ODP Leg 125): evidence for mantle melting and melt-mantle interaction in a suprasubduction zone setting. Journal of Petrology 39, 1577–1618.

Pearce, J.A., Norry, M.J., 1979. Petrogenetic implications of Ti, Zr, Y, and Nb variations in volcanic rocks. Contributions to Mineralogy and Petrology 69, 33–47.

Pearce, J.A., 1982. Trace element characteristics of lavas from destructive plate boundaries. In: Thorpe, R.S. (Ed.), Andesites. Wiley, New York, pp. 525–548.

Pearce, J.A., 1983. Role of the sub-continental lithosphere in magma genesis at active continental margin. In: Hawkesworth, C.J., Norry, M.J. (Eds.), Continental Basalts and Mantle Xenoliths. Shiva Publications, Nantwich, Cheshire, pp. 230–249.

Pearce, J.A., Parkinson, I.J., 1993. Trace element models for mantle melting: application to volcanic arc petrogenesis. Geological Society of London Special Publications 76, 373–403.

Pearce, J.A., 1996. A user's guide to basalt discrimination diagrams. In: Bailes, A.H., Christiansen, E.H., Galley, A.G., Jenner, G.A., Keith, J.D., Kerrich, R., Lentz, D.R., Lesher, C.M., Lucas, S.B., Ludden, J.N., Pearce, J.A., Peloquin, S.A., Stern, R.A., Stone, W.E., Syme, E.C., Swinden, H.S., Wyman, D.A. (Eds.), Trace Element Geochemistry of Volcanic Rocks: Applications for Massive Sulphide Exploration. Short Course Notes, vol. 12. Geological Association of Canada, pp. 79–113.

Pessagno, E.A., Newport, R.L., 1972. A technique for extracting Radiolaria from radiolarian chert. Micropaleontology 18, 231–234.

Pirnia, T., Arai, S., Torabi, G., 2010. Post-deformational impregnation of depleted MORB in Nain lherzolite (Central Iran). Journal of Mineralogical and Petrological Sciences 105, 74–79.

Pirnia, T., Arai, S., Torabi, G., 2013. A better picture of the mantle of the Nain ophiolite inferred from detrital chromian spinels. Journal of Geology 121, 645–661.

Pirnia, T., Arai, S., Tamura, A., Ishimaru, S., Torabi, G., 2014. Sr enrichment in mantle pyroxenes as a result of plagioclase alteration in lherzolite. Lithos 196–197, 198–212.

Pirnia, T., Saccani, E., Arai, S., 2018. Spinel and plagioclase peridotites of the Nain ophiolites (Central Iran): evidence for the incipient stage of oceanic basin formation. Lithos 310–311, 1–19. https://doi.org/10.1016/j.lithos.2018.04.001.

Putirka, K.D., 2008. Thermometers and barometers for volcanic systems. In: Putirka, K.D., Tepley III, F.J. (Eds.), Minerals, Inclusions and Volcanic Processes. Mineralogical Society of America, vol. 69. Reviews in Mineralogy and Geochemistry, Washington DC, pp. 61–120.

Putirka, K.D., Mikaelian, H., Ryerson, F., Shaw, H., 2003. New clinopyroxene-liquid thermobarometers for mafic, evolved, and volatile-bearing lava compositions, with applications to lavas from Tibet and the Snake River Plain, Idaho. American Mineralogist 88, 1542–1554.

Rahmani, F., Noghreyan, M., Khalili, M., 2007. Geochemistry of sheeted dikes in the Nain ophiolite (Central Iran). Ofioliti 32, 119–129.

Rezaei, Z., Noghreyan, M., Saccani, E., 2018. Petrology and geochemistry of sheeted dykes and pillow lavas from the Sabzevar Ophiolite Ophiolitic Mélange (Northeast Iran): New constraints for the Late Cretaceous evolution of the Neo-Tethys Oceanic Basin between the Central Iranian Microcontinent and Eurasia. Ofioliti 43 (2), 147–172. https://doi.org/10.4454/ofioliti.v43i2.461.

Robertson, A.H.F., 2007. Overview of tectonic settings related to the rifting and opening of Mesozoic ocean basins in the Eastern Tethys: Oman, Himalayas and Eastern Mediterranean regions. In: Karner, G.D., Manatschal, G., Pinheiro, L.M. (Eds.), Imaging, Mapping and Modelling Continental Lithosphere Extension and Breakup. Geological Society of London, Special Publication 282, pp. 325–388.

Rolland, Y., Galoyan, G., Bosch, D., Sosson, M., Corsini, M., Fornari, M., Verati, C., 2009. Jurassic Back-arc and hot-spot related series in the Armenian ophiolites-Implications for the obduction process. Lithos 112, 163–187.

Rollinson, H., 2008. The geochemistry of mantle chromitites from the northern part of the Oman ophiolite: inferred parental melt compositions. Contributions to Mineralogy and Petrology 156, 273–288.

Rossetti, F., Nasrabady, M., Vignaroli, G., Theye, T., Gerdes, A., Razavi, M., Moin Vaziri, H., 2010. Early Cretaceous migmatitic mafic granulites from the Sabzevar range (NE Iran): implications for the closure of the Mesozoic peri-Tethyan oceans in central Iran. Terra Nova 22, 26–34.

Saccani, E., Photiades, A., Beccaluva, L., 2008a. Petrogenesis and tectonic significance of IAT magma-types in the Hellenide ophiolites as deduced from the Rhodiani ophiolites (Pelagonian zone, Greece). Lithos 104, 71–84.

Saccani, E., Bortolotti, V., Marroni, M., Pandolfi, L., Photiades, A., Principi, G., 2008b. The Jurassic association of backarc basin ophiolites and calc-alkaline volcanics in the Guevgueli Complex (northern Greece): implication for the evolution of the Vardar Zone. Ofioliti 33, 209–227.

Saccani, E., Delavari, M., Beccaluva, L., Amini, S., 2010. Petrological and geochemical constraints on the origin of the Nehbandan ophiolitic complex (eastern Iran): implication for the evolution of the Sistan Ocean. Lithos 117, 209–228.

Saccani, E., Allahyari, K., Rahimzadeh, B., 2014. Petrology and geochemistry of mafic magmatic rocks from the Sarve-Abad ophiolites (Kurdistan region, Iran): evidence for interaction between MORB-type asthenosphere and OIB-type components in the southern Neo-Tethys Ocean. Tectonophysics 621, 132–147.

Saccani, E., Dilek, Y., Marroni, M., Pandolfi, L., 2015. Continental margin ophiolites of Neotethys: remnants of ancient ocean-continent transition zone (OCTZ) lithosphere and their geochemistry, mantle sources and melt evolution patterns. Episodes 38, 230–249. https://doi.org/10.18814/epiiugs/2015/v38i4/82418.

Saccani, E., Tassinari, R., 2015. The role of MORB and SSZ magma-types in the formation of Jurassic ultramafic cumulates in the Mirdita ophiolites (Albania) as deduced from chromian spinel and olivine chemistry. Ofioliti 40, 37–56.

Saccani, E., Delavari, M., Dolati, A., Marroni, M., Pandolfi, L., Chiari, M., Barbero, E., 2017a. New insights into the geodynamics of Neo-Tethys in the Makran area: evidence from age and petrology of ophiolites from the Coloured Mélange Complex (SE Iran). Gondwana Research 62, 306–327. https://doi.org/10.1016/j.gr.2017.07.013.

Saccani, E., Dilek, Y., Photiades, A., 2017b. Time-progressive mantle-melt evolution and magma production in a Tethyan marginal sea: a case study of the Albanide-Hellenide ophiolites. Lithosphere 10, 35–53. https://doi.org/10.1130/L602.1.

Saffer, D.M., Tobin, H.J., 2011. Hydrogeology and mechanics of subduction zone forearcs: fluid flow and pore pressure. Annual Review of Earth and Planetary Sciences 39, 157–186.

Sengör, A.M.C., 1990. A new model for the Late Paleozoic-Mesozoic tectonic evolution of Iran and implications for Oman. In: Robertson, A.H.F., Searle, M.P., Ries, A.C. (Eds.), The Geology and Tectonics of the Oman Region, vol. 49. Geological Society London, Special Publications, pp. 797–831.

Please cite this article as: Pirnia, T et al., Cretaceous tectonic evolution of the Neo-Tethys in Central Iran: Evidence from petrology and age of the Nain-Ashin ophiolitic basalts, Geoscience Frontiers, https://doi.org/10.1016/j.gsf.2019.02.008

Shahabpour, J., 2005. Tectonic evolution of the orogenic belt in the region located between Kerman and Neyriz. Journal of Asian Earth Sciences 24, 405–417.
Shafaii Moghadam, H., Rahgoshay, M., Whitechurch, H., 2008. Mesozoic back-arc extension in the active margin of the Iranian continental block: constraints from age and geochemistry of the mafic lavas. Ofioliti 33, 95–103.
Shafaii Moghadam, H., Whitechurch, H., Rahgoshay, M., Monsef, L., 2009. Significance of Nain-Baft ophiolite belt (Iran): short-lived, transtensional Cretaceous back-arc oceanic basins over the Tethyan subduction zone. Comptes Rendus Geoscience 341, 1016–1028.
Sharkovski, M., Susov, M., Krivyakin, B., Morozov, L., Kiristaev, V., Romanko, E., 1984. Geology of the Anarak Area (Central Iran). Explanatory Text of the Anarak Quadrangle Map 1:250000. Report No. 19. Geological Survey of Iran and Moscow, V/O "Technoexport", Tehran, p. 143.
Shirdashtzadeh, N., Torabi, G., Arai, S., 2010. Metamorphism and metasomatism in the Jurassic Nain ophiolite melange, Central Iran. Neues Jahrbuch für Geologie und Paläontologie Abhandlungen 255, 255–275.
Shirdashtzadeh, N., Torabi, G., Arai, S., 2011. Two Mesozoic oceanic phases recorded in the basic and metabasic rocks of the Nain and Ashin-Zavar ophiolitic melanges (Isfahan Province, Central Iran). Ofioliti 36, 191–205.
Shirdashtzadeh, N., Kachovich, S., Aitchison, J.C., Samadi, R., 2015. Mid-cretaceous radiolarian faunas from the Ashin ophiolite (western Central-East Iranian microcontinent). Cretaceous Research 56, 110–118.
Shojaat, B., Hassanipak, A.A., Mobasher, K., Ghazi, A.M., 2003. Petrology, geochemistry and tectonics of the Sabzevar ophiolite, North Central Iran. Journal of Asian Earth Sciences 21, 1053–1067.
Stevens, R.E., 1944. Composition of some chromites of the western Hemisphere. American Mineralogist 29, 1–34.
Stöcklin, J., 1974. Northern Iran: Alborz mountain. In: Spencer, A.M. (Ed.), Mesozoic-Cenozoic Orogenic Belts, Data for Orogenic Studies, vol. 4. Geological Society of London Special Publications, pp. 213–234.
Stoneley, R., 1975. On the origin of ophiolite complexes in the southern Tethys region. Tectonophysics 25, 303–322.
Sun, S.S., McDonough, W.F., 1989. Chemical and isotopic-systematics of oceanic basalts: implications for mantle composition and processes. In: Saunders, A.D., Norry, M.J. (Eds.), Magmatism in Ocean Basins, vol. 42. Geological Society of London, Special Publications, pp. 313–345.
Takin, M., 1972. Iranian geology and continental drift in the Middle East. Nature 235, 147–150.
Tankut, A., Dilek, Y., Önen, P., 1998. Petrology and geochemistry of the Neo-Tethyan volcanism as revealed in the Ankara melange, Turkey. Journal of Volcanology and Geothermal Research 85, 265–284.
Taylor, S.R., McLennan, S.M., 1985. The Continental Crust: its Composition and Evolution: an Examination of the Geochemical Record Preserved in Sedimentary Rocks. Blackwell Scientific Publication, Oxford, p. 312.
Torabi, G., 2004. Petrology of Anarak Area Ophiolites (NE of Isfahan Province, Iran) (PhD thesis). Tarbiat Modarres University, p. 240.
Torabi, G., Abdullahi, E., Shirdashtzadeh, N., 2008. Application of mineral and whole rock analysis in identification of petrogenesis of pillow lavas in the Nain ophiolite. Iranian Journal of Crystallography and Mineralogy 16, 295–312 (in Persian with English abstract).
Torabi, G., Arai, S., Koepke, J., 2011a. Metamorphosed mantle peridotites from Central Iran (Jandaq area, Isfahan province). Neues Jahrbuch für Geologie und Paläontologie-Abhandlungen 261, 129–150.
Torabi, G., Shirdashtzadeh, N., Arai, S., Koepke, J., 2011b. Paleozoic and Mesozoic ophiolites of Central Iran: amphibolites from Jandaq, Posht-e-Badam, Nain and Ashin ophiolites. Neues Jahrbuch für Geologie und Paläontologie Abhandlungen 262, 227–240.
Valsami, E., Cann, J.R., 1992. Mobility of rare earth elements in zones of intense hydrothermal alteration in the Pindos ophiolite, Greece. In: Parson, L.M., Murton, B.J., Browning, P. (Eds.), Ophiolites and Their Modern Oceanic Analogues, vol. 60. Geological Society of London, Special Publications, pp. 219–232.
Winchester, J.A., Floyd, P.A., 1977. Geochemical discrimination of different magma series and their differentiation products using immobile elements. Chemical Geology 20, 325–343.
Whitney, D.L., Bernard, W.E., 2010. Abbreviations for names of rock-forming minerals. American Mineralogist 95, 185–187. https://doi.org/10.2138/am.2010.3371.
Workman, R.K., Hart, S.R., 2005. Major and trace element composition of the depleted MORB mantle (DMM). Earth and Planetary Science Letters 231, 53–72, 2005.
Yuan, C., Sun, M., Zhou, M.F., Xiao, W., Zhou, H., 2005. Geochemistry and petrogenesis of the Yishak Volcanic Sequence, Kudi ophiolite, West Kunlun (NW China): implications for the magmatic evolution in a subduction zone environment. Contributions to Mineralogy and Petrology 150, 195–211.
Zanchetta, S., Malaspina, N., Zanchi, A., Benciolini, L., Martin, S., Javadi, H.R., Kouhpeyma, M., 2017. Contrasting subduction-exhumation paths in the blueschists of the Anarak metamorphic complex (Central Iran). Geological Magazine 155, 316–334.
Zanchi, A., Malaspina, N., Zanchetta, S., Berra, F., Benciolini, L., Bergomi, M., Cavallo, A., Javadi, H.R., Kouhpeyma, M., 2015. The Cimmerian accretionary wedge of Anarak, Central Iran. Journal of Asian Earth Sciences 102, 45–72.
Zhou, M.F., Robinson, P.T., Malpas, J., Li, Z., 1996. Podiform chromitites in the Luobusa ophiolite (southern Tibet): implications for melt-rock interaction and chromite segregation in the upper mantle. Journal of Petrology 37, 3–21.

Please cite this article as: Pirnia, T et al., Cretaceous tectonic evolution of the Neo-Tethys in Central Iran: Evidence from petrology and age of the Nain-Ashin ophiolitic basalts, Geoscience Frontiers, https://doi.org/10.1016/j.gsf.2019.02.008